4

Advanced Base Isolation Systems for Light Weight Equipments

Chong-Shien Tsai
Department of Civil Engineering, Feng Chia University, Taichung, Taiwan

1. Introduction

This chapter is intended to introduce the earthquake proof technology particularly in the area of base isolation systems that have been used to protect light weight structures, such as motion sensitive equipment, historic treasures, and medical instruments, etc., from earthquake damage. This chapter presents theoretical background, experimental studies, numerical analyses, and the applications of the advanced isolation systems consisting of rolling- and sliding-type isolation systems for light weight structures. The efficiency of these isolators in reducing the seismic responses of light weight equipment was also investigated in this study. In addition, the results from theoretical and experimental studies for these isolators are compared and discussed.

1.1 General background

One of the greatest casualties in recorded history is the Huaxian earthquake that occurred in China in 1556, causing over 830,000 deaths (Kanamori, 1978). The Tangshan great earthquake that struck the northeastern part of China in 1976 killed 242,769 people, according to official sources, although some estimates of the death toll are as high as 650,000 (Kanamori, 1978). The Mw 7.0 earthquake (Eberhard et al., 2010) that struck the Republic of Haiti on January 12, 2010, resulted in a death toll, as reported by the Government of Haiti, that exceeds 217,000, with an additional 300,000 people injured. The earthquake damaged nearly 190,000 houses, of which 105,000 were completely destroyed, and left long term suffering for the residents of the country. The moment magnitude 9.0 Tohoku earthquake (Takewakin et al., 2011) that struck eastern Japan on March 11, 2011, is one of the most five powerful earthquakes in the world since modern measurements began in 1900, killing more than 20,000 people and causing huge damage and economic loss that cannot be ignored.

Traditionally designed structures have used the strength and ductility of their structural members to resist the seismic forces or dissipate earthquake induced energy. However, many past earthquakes have proven that structures collapse or lose their functionality when the ductility capacity of the structures is consumed during the earthquake. Even if the structures survive earthquakes through excellent designs to provide more strength or ductility to the structures, the vibration sensitive equipment located in the structures may still lose its functionality due to floor accelerations.

Several techniques exist to minimize earthquake effects on structures, such as light-weight structure design, improving the ductility capacities of structures, and structural control (earthquake proof technology), etc. Structural control technology has been recognized as an effective tool in seismic mitigation, and can be classified as active, passive, hybrid and semi-active controls, which can be clarified by the following equation:

$$M\ddot{u}+C\dot{u}+Ku=-MB\ddot{u}_g+F(\ddot{u},\dot{u},u,t) \tag{1}$$

where M, C, and K are the mass, the damping, and stiffness matrices, respectively, of a structure, which are the natural characteristics of a structure; $\ddot{u}$, $\dot{u}$ and u denote the vectors of the relative acceleration, velocity, and displacement with respect to supports, respectively, which are structural responses during earthquakes; $\ddot{u}_g$ is the ground acceleration; B is the displacement transformation matrix; and $F(\ddot{u},\dot{u},u,t)$ depicts the control force that is an external force provided by various types of power and control systems.

Active control technology has a control force used to activate the control system. The control force is generated through the control signal which is based on the results calculated from the measured responses of the structure and the specified control algorithm. The structural responses can be lessened by changing its characteristic through the control force in the second term on the right hand side of Eq. (1) which could be proportional to the measured displacement, velocity and acceleration of the structure during earthquakes. From a mathematical point of view, we can then move the control force from the right hand side to the left hand side of Eq. (1) to combine with the corresponding terms depending on the values of the control fore proportional to. As a result, the mass, damping, and stiffness matrices of a structure are modified by the control force, but not by an actual device.

In the passive control, there is no external control force, $F(\ddot{u},\dot{u},u,t)$, in the system, which means that there is no second term on the right hand side of Eq. (1). The mass, damping, or stiffness which are the first three terms on the left hand side are modified by adding actual devices to the structure (Soong and Dragush, 1997; Takewakin, 2009). The device used to modify the mass matrix is named the tuned mass damper. Any actual devices used to modify the second and third terms on the left hand side of Eq. (1) are called energy absorbing systems (or dampers). A device such as a fluid damper producing an internal force that is strongly dependent on the relative velocity between the two ends of the device is called a velocity dependent device (damper). On the other hand, a device such as a friction and yielding dampers producing an internal force that is strongly dependent on the relative displacement between the two ends of the device is called a displacement dependent device (damper). Usually, the velocity dependent device produces minimum internal forces at the moments of maximum displacement due to zero velocity, which means that this type device provides no damping effect to the structure while the structure deforms at critical moments of earthquakes. On the other hand, the displacement dependent device produces maximum internal forces at maximum displacements. This means that this type device can provide maximum damping effect at the moments of maximum displacement and immediately reduce the structural responses at the most critical time of structural responses. The discussions of the advantages and disadvantages of these two types of devices are out of the scope of this chapter.

A system called the base (seismic) isolation system inserts a soft layer or device (base isolator) between the structure and its foundation to isolate earthquake-induced energy trying to penetrate into the structure, thereby protecting the structure from earthquake damage (Skinner et al., 1993; Naeim and Kelly, 1999). A base isolation system is used to minimize the seismic force which is the first term on the right hand side of Eq. (1) in two ways: (i) by reflecting the seismic energy by lengthening the natural period of the entire system including the structure and the base isolator and (ii) by absorbing the seismic energy through the hysteretic loop of the isolator displacement and the force induced in the isolator. The combination of the active and passive control is called hybrid control, which also needs a large control force for controlling structural responses. By contrast, semi-active control uses substantially smaller control force in the manner of an on and off switch to improve the efficiency of the passive control system through an active control algorithm, but not massive control force. In conclusion, structural control technology protects structures through mechanisms that are used to prohibit the seismic energy from transmitting into major members such as the beams, columns and walls of a structure, which are used for supporting structural weight.

In the past, there have been a lot of papers and reports concerning the use of vibration isolation technology to increase the precision of machines by isolating vibration sources resulting from the environment, such as moving vehicles, or for improving human comfort by isolating vibration sources that result from machines and moving vehicles (Rivin, 2003). Recently, the isolation technology has been acknowledged as an effective technique to promote the earthquake resistibility of the structures by controlling structural responses during earthquakes on the basis of theoretical and experimental results and earthquake events (Naeim and Kelly, 1999). Several theoretical studies have been made on the applications of the base isolation technology to critical equipment in seismic mitigation (Alhan and Gavin, 2005; Chung et al., 2008). However, little attention has been given to the experimental study of the efficiency of base isolation on the protection of vibration sensitive equipment in the events of earthquakes, especially for experimental investigations under tri-directional seismic loadings (Tsai et al., 2005b, 2007, 2008a; Fan et al., 2008).

This chapter is aimed at the seismic isolation, especially for the equipments in hospitals and facilities of emergency departments used for saving peoples' lives. These are of extreme importance and should be kept functional during and after earthquakes.

1.2 Background of rolling types of bearings

To the best of the author's knowledge, the isolation system with doubled spherical concave surfaces and a rolling ball located between these two concave surfaces was first patented by Touaillon in 1870, as shown in Fig. 1(a). Several similar isolation systems with a ball located between two spherical concave surfaces were also proposed (Schär, 1910; Cummings, 1930; Bakker, 1935; Wu, 1989), as shown in Figs. 1(b)-1(e). In 1997, Kemeny propounded a ball-in-cone seismic isolation bearing that includes two conical concave surfaces and a ball seated between the conical surfaces, as shown in Fig. 1(f). The dynamic behavior of the ball-in-cone isolation system has been investigated (Kasalanati et al., 1997). In addition, Cummings (1930) also proposed a seismic isolation system with a rolling rod of a cylinder sandwiched between two concave surfaces, as shown in Fig. 1(c). Lin and Hone (1993), Tsai et al. (2006b) and M. H. Tsai et al. (2007) conducted research on the effectiveness of this type of base isolation system in seismic mitigation, as shown in Figs. 2(a) and 2(b). Kim (2004) proposed

a seismic isolation system that has rollers of a bowling shape to roll in the friction channel, as shown in Fig. 2(c). Tsai (2008a, b) revealed seismic isolation systems each consisting of shafts rolling in the concave slot channels, as shown in Figs. 2(a) and 2(d). These devices are capable of resisting the uplift while the vertical force in the isolator becomes negative under severe earthquakes.

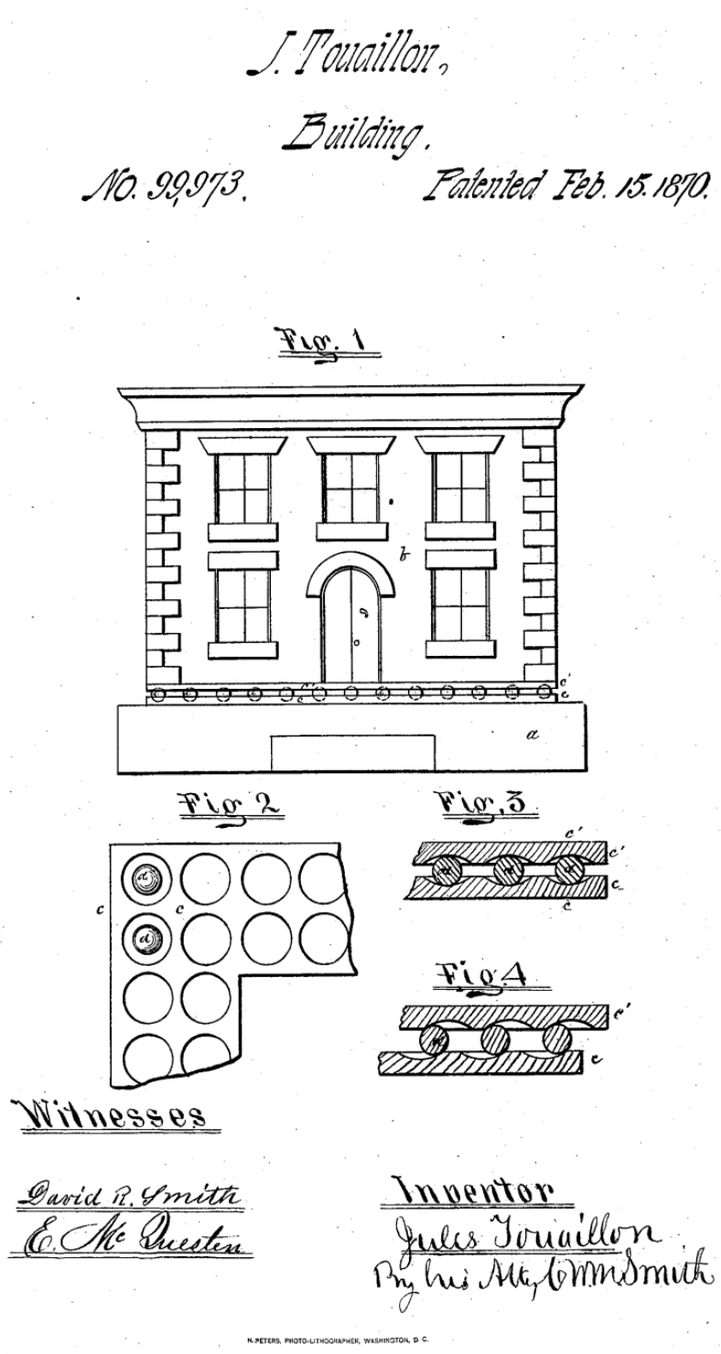
J. Touaillon,

Building.

No. 99,973. Patented Feb. 15. 1870.

Fig. 1

Fig. 2

Fig. 3

Fig. 4

Witnesses

David R. Smith

E. McQuesten

Inventor

Jules Touaillon

By his Atty's Wm. Smith

N. PETERS, PHOTO-LITHOGRAPHER, WASHINGTON, D. C.

Fig. 1(a). Touaillon's original patent (1870)

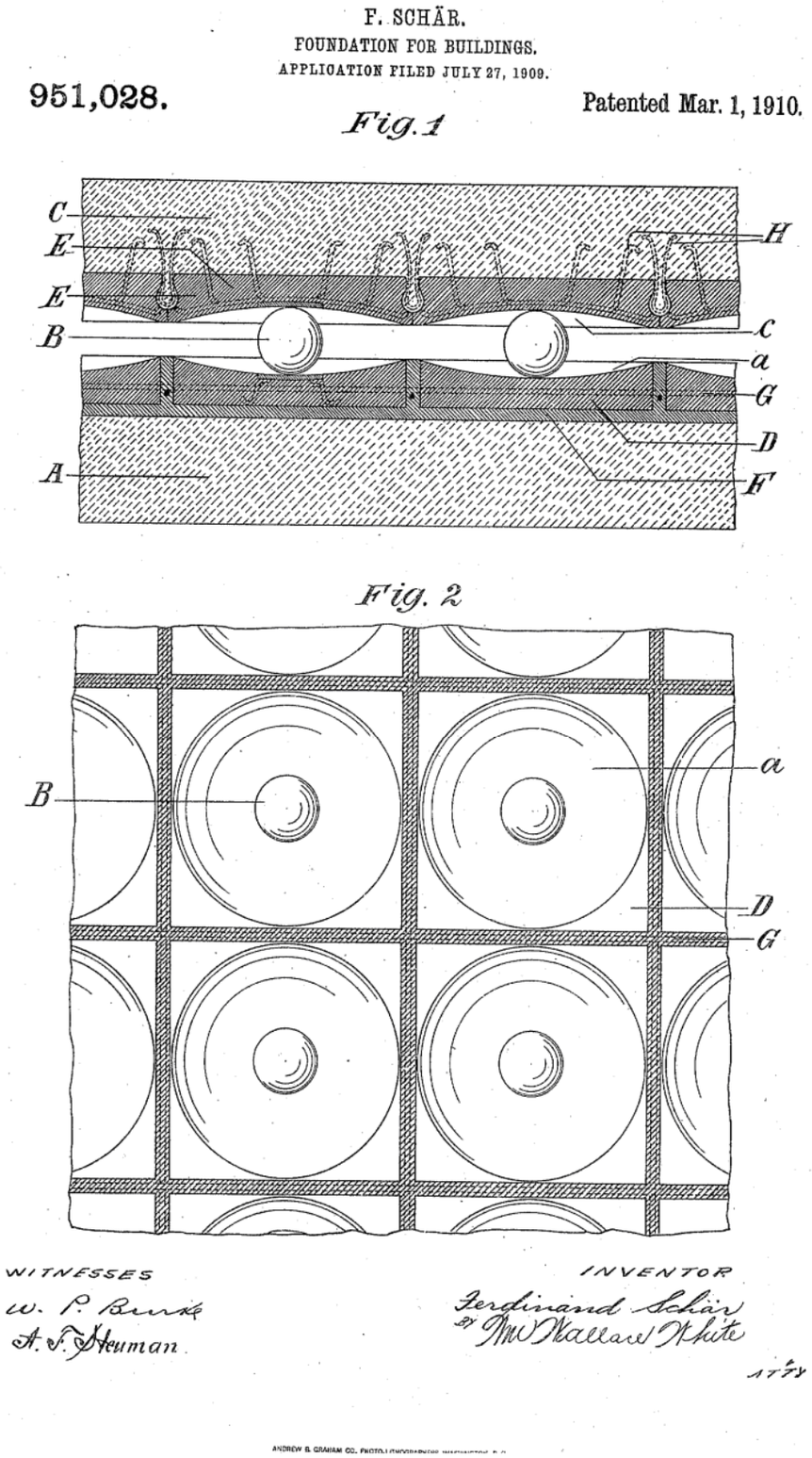
F. SCHÄR.
FOUNDATION FOR BUILDINGS.
APPLICATION FILED JULY 27, 1909.

951,028. Patented Mar. 1, 1910.

Fig. 1

Fig. 2

WITNESSES
W. P. Burke
A. J. Heuman

INVENTOR
Ferdinand Schär
by Wm Wallace White
Atty

ANDREW B. GRAHAM CO. PHOTO-LITHOGRAPHERS WASHINGTON, D. C.

Fig. 1(b). Schär's original patent (1910)

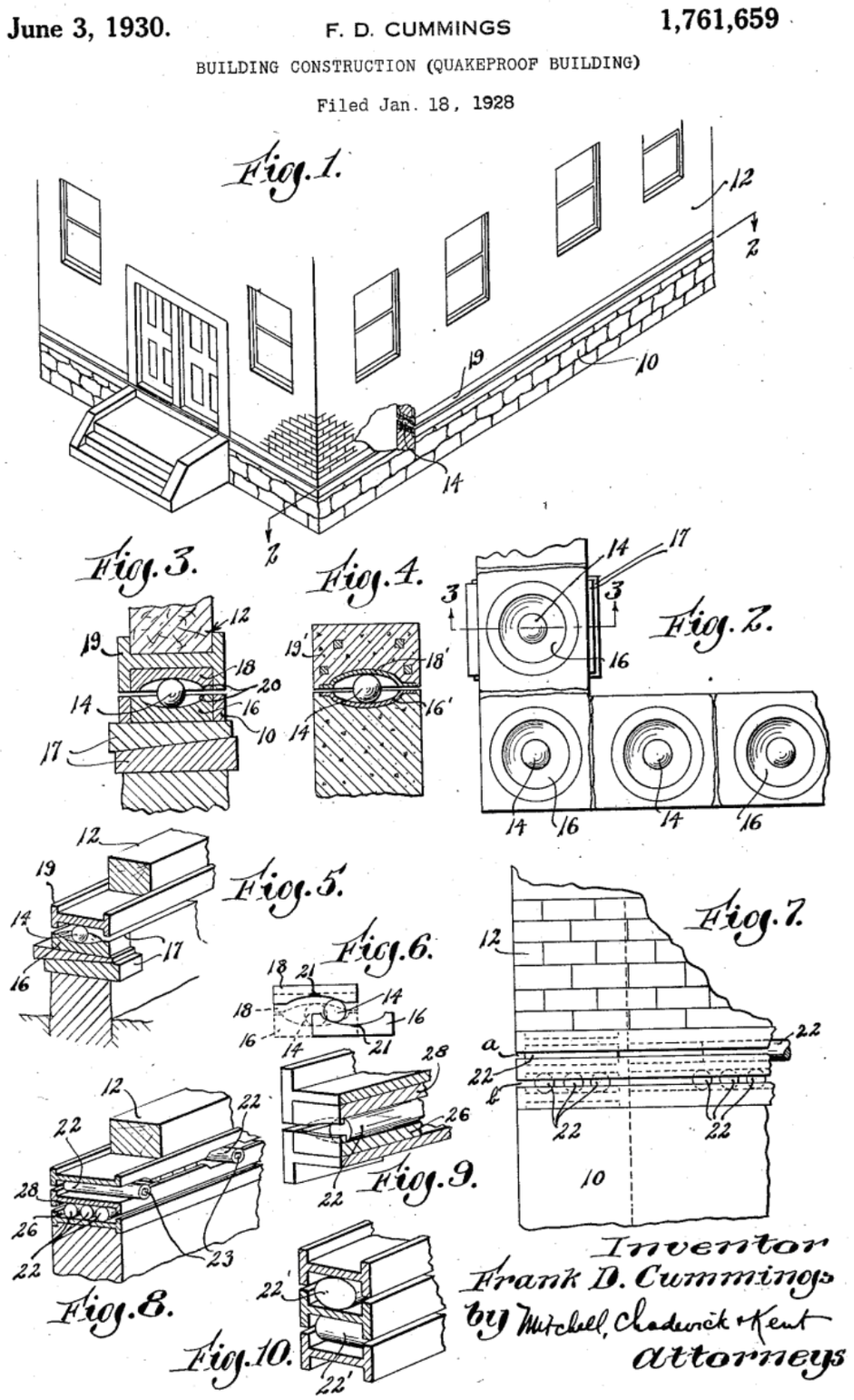

Fig. 1(c). Cummings' original patent (1930)

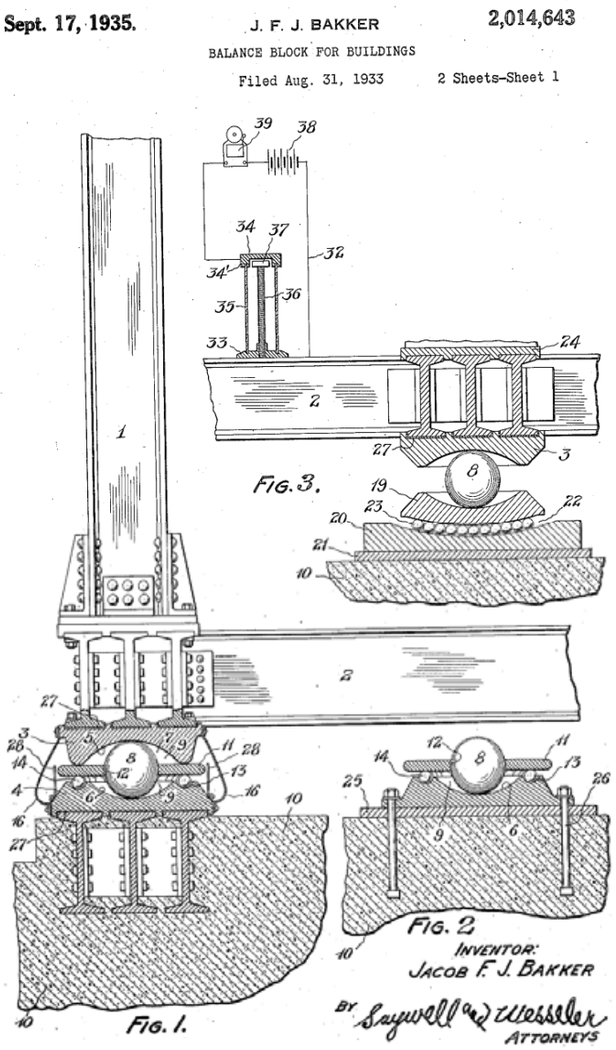

Fig. 1(d). Bakker's original patent (1935)

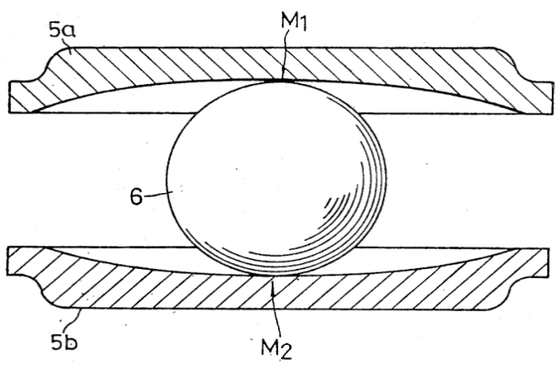

Fig. 1(e). Wu's original patent (1989)

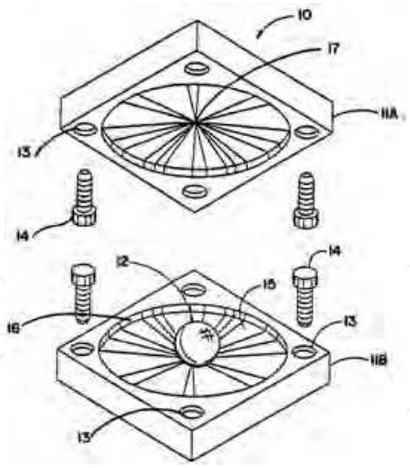

Fig. 1(f). Kemeny's original patent (1997)

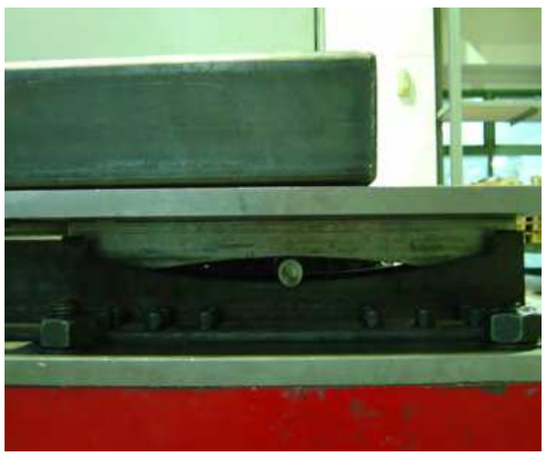

Fig. 2(a). Rolling rod isolation system

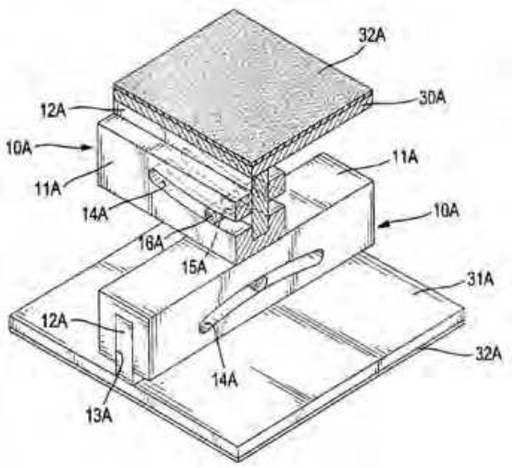

Fig. 2(b). Tsai's original patent (2008a)

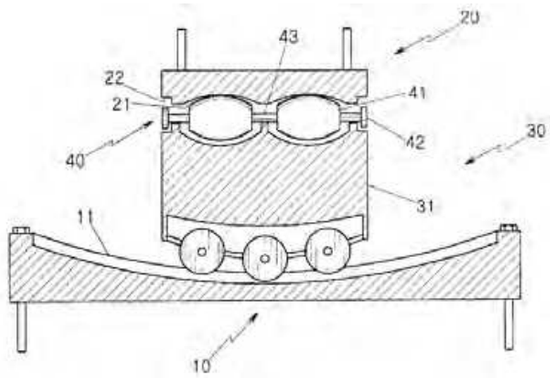

Fig. 2(c). Kim's original patent (2004)

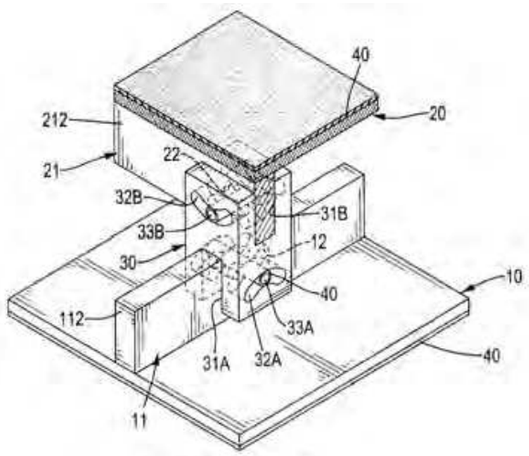

Fig. 2(d). Tsai's original patent (2008b)

The isolation system with two concave surfaces and a rolling ball (Touaillon, 1870; Wu, 1989; Kemeny, 1997) possesses some shortcomings even under small loadings like equipment and medical instruments, such as negligible damping provided by the system, a highly concentrated stress resulted from the weight of the equipment on the rolling ball and the concave surfaces due to the small contact area, and scratches and damage to the concave surfaces caused by the ball rolling motions during earthquakes. The rolling ball has a tendency to move even under environmental loadings such as human activities during regular services. In addition, the bearing size is large because of the large bearing displacements under seismic loadings due to insufficient damping provided by the rolling motion of the ball on the concave surfaces in the system.

To supply more damping to the isolation system and simultaneously reduce the bearing size as a consequence of smaller bearing displacements during earthquakes, Tsai et al. (2006a) proposed a ball pendulum system (BPS). As shown in Figs. 3(a) and 3(b), this system comprises two spherical concave surfaces and a steel rolling ball covered with a special damping material to provide horizontal and vertical damping to tackle the problems mentioned above. A series of shaking table tests conducted by Tsai et al. (2006a) have proven that the BPS isolator can enhance the seismic resistibility of vibration sensitive equipment under severe earthquakes with smaller displacements compared to an isolation

system with negligible damping. However, the special material covering the steel ball that supports the weight of the vibration sensitive equipment for a long period of time in its service life span might result in permanent deformation due to plastic deformation in the damping material. It may damage or flat the contacting surface of the special damping material after sustaining a certain period of service loadings and affect the isolation efficiency.

Fig. 3(a). Open-up view of ball pendulum isolation system

Fig. 3(b). Test set-up for ball pendulum isolation system

An alternative approach for increasing damping and lessening the isolator displacement is to add a damping device to the isolation system (Fan et al., 2008). Fathali and Filiatrault (2007) presented a spring isolation system with restraint which is a rubber snubber to play a role of displacement restrainer to limit the isolator displacement. In general, the displacement restrainer will involve impact mechanisms as a result of contact made with isolated equipment, which lead to amplified acceleration responses and large dynamic forces.

To increase damping for a rolling bearing and to prolong the service life of a bearing, an isolation system called the static dynamics interchangeable–ball pendulum system (SDI-BPS) shown as Figures 4(a) and 4(b) was proposed by Tsai et al. (2008a). The SDI-BPS system consists of not only two spherical concave surfaces and a steel rolling ball covered with a special damping material to provide supplemental damping and prevent any damage and scratches to the concave surfaces during the dynamic motions induced by earthquakes but also several small steel balls that are used to support the static weight to prevent any plastic deformation or damage to the damping material surrounding the steel rolling ball during the long term of service loadings. Because the concave surfaces are protected by the damping material covering the steel ball from damage and scratches, they may be designed as any desired shapes in geometry, which can be spherical, conical or

concave surfaces with variable radii of curvature. The natural period of the SDI-BPS isolator depends only on the radii of curvature of the upper and lower concave surfaces, but not a function of the vertical loading (static weight). It can be designed as a function of the isolator displacement, and predictable and controllable for various purposes of engineering practice.

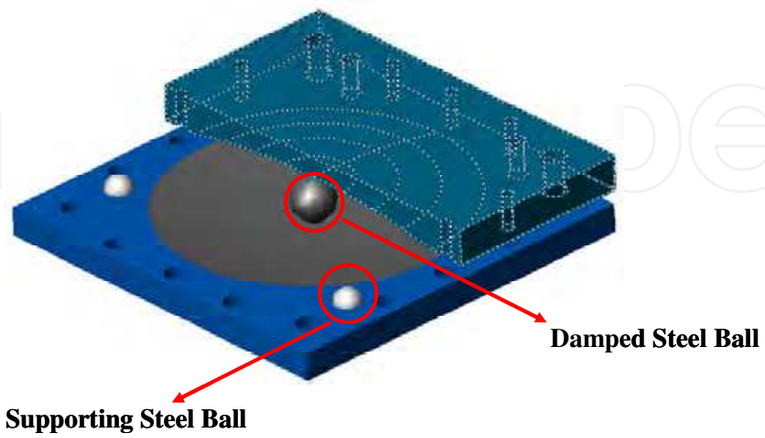

Fig. 4(a). Exploded perspective view of static dynamics interchangeable–ball pendulum system (SDI-BPS)

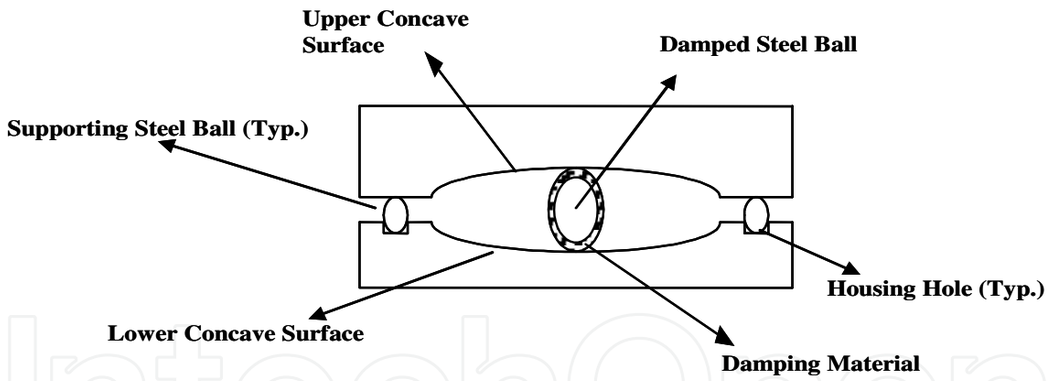

Fig. 4(b). Cross-sectional view of SDI-BPS

1.3 Background of sliding types of bearings

Most sliding types of isolation systems are suitable not only for light weight structures such as equipment and medical instruments but also for very heavy structures such as buildings and bridges. These types of bearings provide damping through frictional mechanism between sliding surfaces. As shown in Fig. 5(a), Penkuhn (1967) proposed a sliding isolation system including a concave sliding surface and a universal joint to accommodate the rotation resulted from the superstructure and the sliding motion of the universal joint, and suggested that the superstructure be supported by a rigid supporting base which was in turn supported by three proposed isolation bearings. Zayas (1987) and Zayas et al. (1987)

proposed a friction pendulum system (FPS) with a concave sliding surface and an articulated slider, as shown in Figs 5(b) and 5(c). Through extensive experimental and numerical studies, the FPS isolator has proven to be an efficient device for reducing the seismic responses of structures (Zayas et al., 1987; Al-Hussaini et al., 1994).

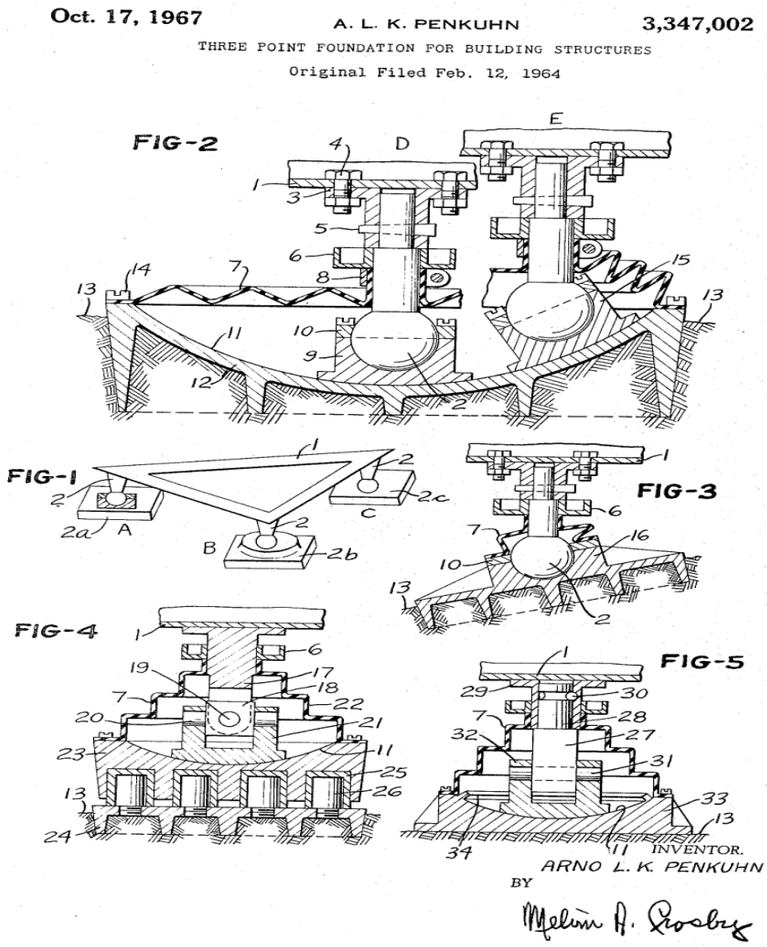

Fig. 5(a). Penkuhn's original patent (1967)

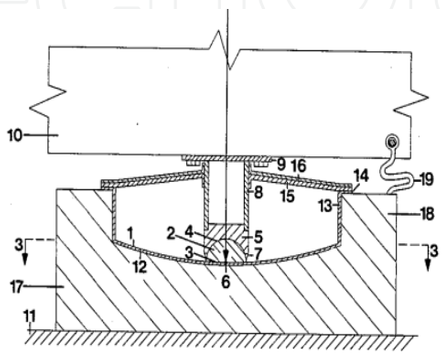

Fig. 5(b). Cross-sectional view of the friction pendulum system

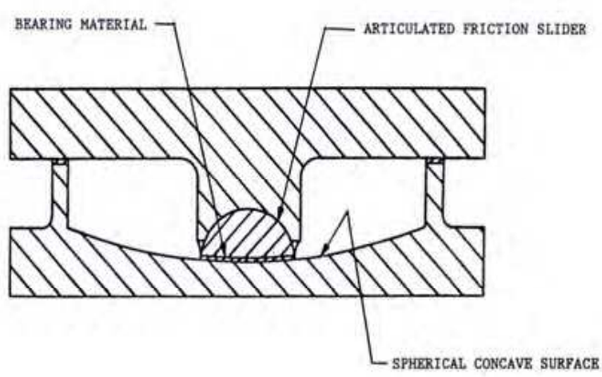

Fig. 5(c). Zayas's original patent (1987)

To avoid the possibility of resonance of the isolator with long predominant periods of ground motions, Tsai et al. (2003a) presented an analytical study for a variable curvature FPS (VCFPS). In order to enhance the quakeproof efficiency and reduce the size of the FPS isolator, Tsai (2004a,b) and Tsai et al. (2003b, 2005a,b, 2006c) proposed a sliding system called the multiple friction pendulum system (MFPS) with double concave sliding surfaces and an articulated slider located between the concave sliding surfaces, as shown in Figs. 6(a)-6(f). Based on this special design, the displacement capacity of the MFPS isolator is double of the FPS isolator that only has a single concave sliding surface, and the bending moment induced by the sliding displacement for the MFPS isolator is an half of that for the FPS isolator. Moreover, the fundamental frequency is lower than that of the FPS as a result of the series connection of the doubled sliding surfaces in the MFPS isolation system, and the bearing is a completely passive apparatus, yet exhibits adaptive stiffness and adaptive damping by using different coefficients of friction and radii of curvature on the concave sliding surfaces to change the stiffness and damping to predictable values at specifiable and controllable displacement amplitudes. Hence, the MFPS device can be given as a more effective tool to reduce the seismic responses of structures even subjected to earthquakes with long predominant periods, and be more flexible in design for engineering practice. In addition, Fenz and Constantinou (2006) conducted research and published their results on this type of base isolation system with double sliding surfaces. Kim and Yun (2007) reported the seismic response characteristics of bridges using an MFPS with double concave sliding interfaces.

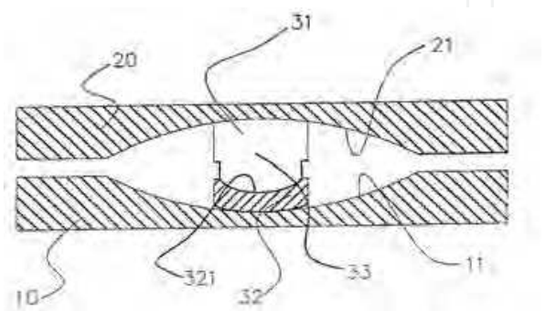

Fig. 6(a). Tsai's original patent (2004a)

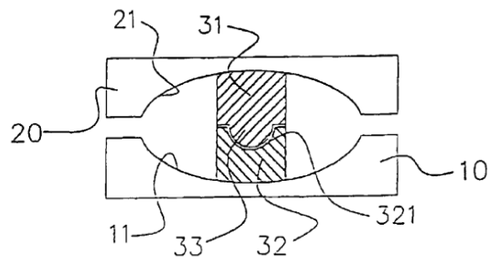

Fig. 6(b). Tsai's original patent (2004a)

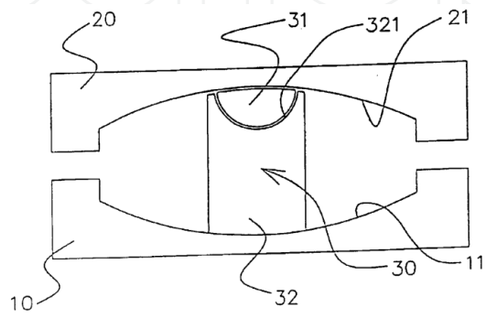

Fig. 6(c). Tsai's original patent (2004a)

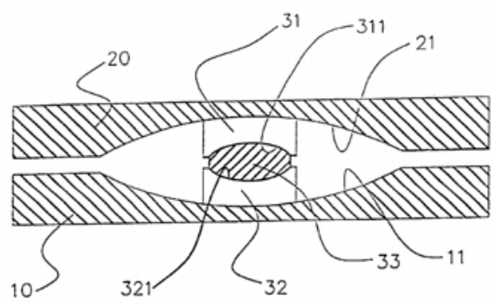

Fig. 6(d). Tsai's original patent (2004b)

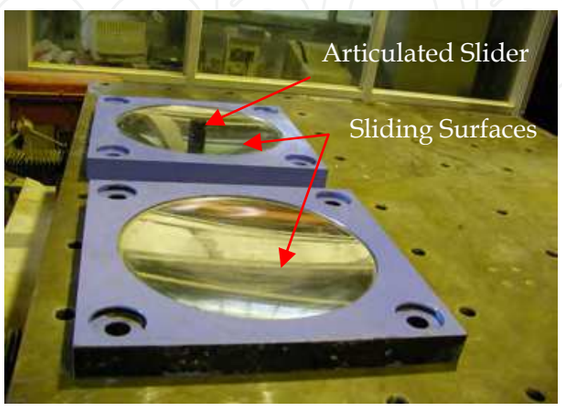

Fig. 6(e). Open-up view of MFPS isolator

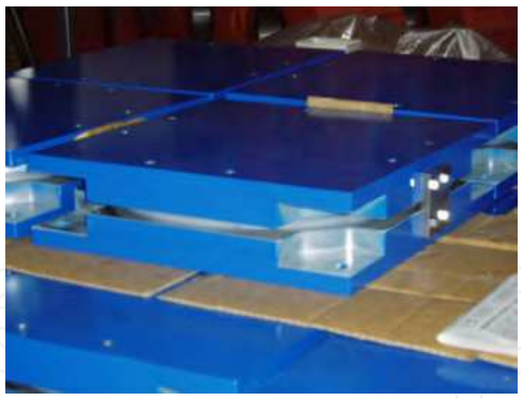

Fig. 6(f). Assembled MFPS isolator

Furthermore, Tsai (2003) proposed several other types of MFPS isolators, as shown in Figs. 7(a)-7(f), each with multiple sliding interfaces, which essentially represent that each FP isolation system above and below the slider has multiple sliding interfaces connected in series (Tsai et al., 2008b, 2010a). Fenz and Constantinou (2008a, b) published their research on the characteristics of an MFPS isolator with four sliding interfaces under unidirectional loadings. Morgan and Mahin (2008, 2010) investigated the efficiency of an MFPS isolator with four concave sliding interfaces on seismic mitigation of buildings. As shown in Figs. 7(g) and 7(h), Tsai et al. (2010a, b) proposed an MFPS isolator with numerous sliding interfaces (any number of sliding interfaces). As explained earlier, these types of bearings, each having N number of sliding interfaces, possess adaptive features of stiffness and damping by adopting different coefficients of friction and radii of curvature on the concave sliding surfaces to result in changeable stiffness and damping at specified displacement amplitudes. Tsai et al. (2011a) published experimental investigations on the earthquake performance of these types of friction pendulum systems. The efficiency of the MFPS isolator with multiple sliding interfaces in mitigating structural responses during earthquakes has been proven through a series of shaking table tests on a full scale steel structure.

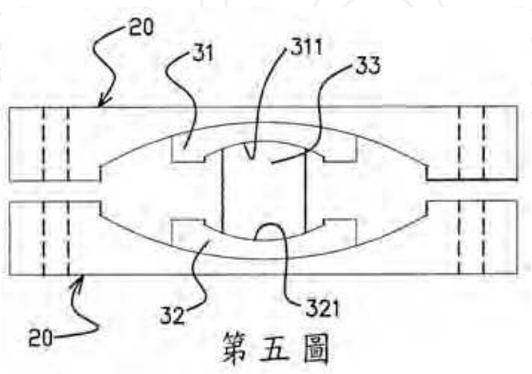

Fig. 7(a). Tsai's original patent (2003)

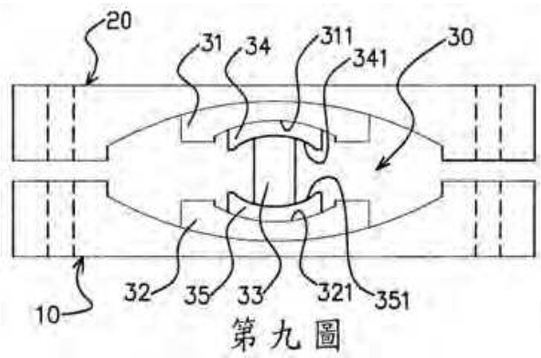

Fig. 7(b). Tsai's original patent (2003)

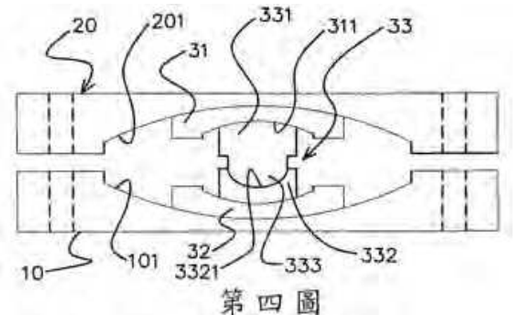

Fig. 7(c). Tsai's original patent (2003)

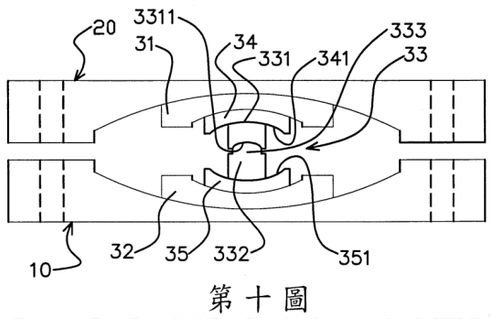

Fig. 7(d). Tsai's original patent (2003)

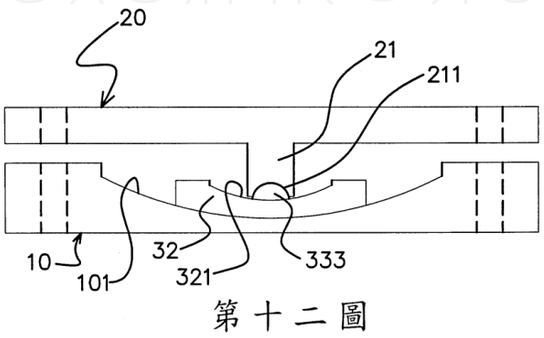

Fig. 7(e). Tsai's original patent (2003)

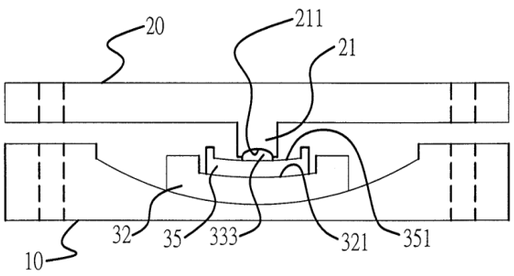

第二十圖

Fig. 7(f). Tsai's original patent (2003)

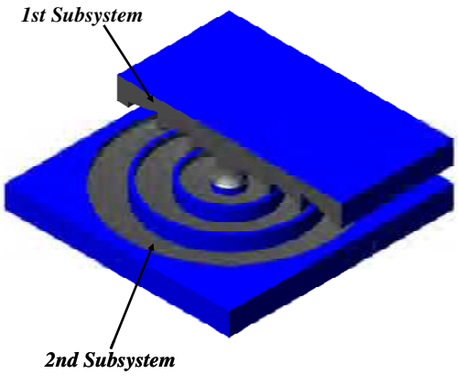

Fig. 7(g). Exploded view of MFPS isolator with six sliding surfaces

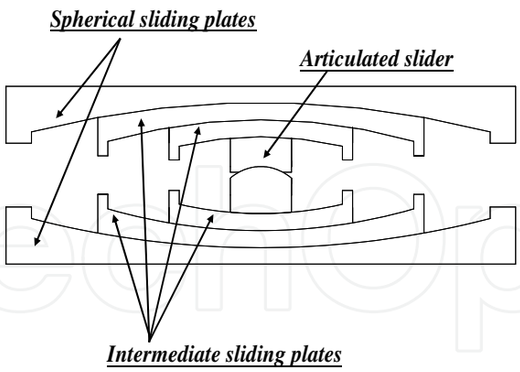

Fig. 7(h). Cross-sectional view of MFPS isolator with six sliding surfaces

An isolation system, as shown in Fig. 8(a) and called the XY-FP isolator, consisting of two orthogonal concave beams interconnected through a sliding mechanism has been published by Roussis and Constantinou (2005). The FP isolator (XY-FP) possesses the uplift-restraint property by allowing continuous transition of the bearing axial force between compression and tension, and has different frictional interface properties under compressive and tensile normal force in the isolator. A device, as shown Fig. 8(b), similar to the design concept but without the uplift-restraint property was also proposed by Tsai (2007). This device has an

articulated slider seated between the FP bearings in the X and Y directions to accommodate the rotation as a result of sliding motion of the articulated slider and to maintain the isolated structure standing vertically during earthquakes.

Fig. 8(a). X-Y (Adatped from Roussis and Constantinou 2005)

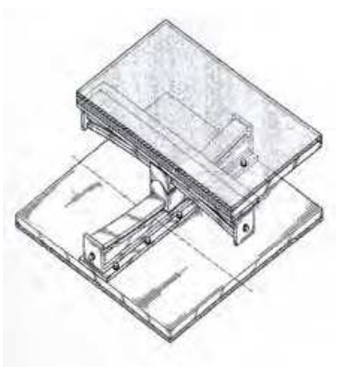

Fig. 8(b). Tsai's original patent (2007)

Tsai et al. (2010c) proposed a trench friction pendulum system (TFPS), as shown in Figs. 9(a) and 9(b), that consists of one trench concave surface in each of two orthogonal directions, and an articulated slider situated between the trench concave surfaces to accommodate the rotation induced by the sliding motion of the slider. The TFPS possesses independent characteristics such as the natural period and damping effect in two orthogonal directions, which can be applied to a bridge, equipment or a structure with considerably different natural periods in two orthogonal directions.

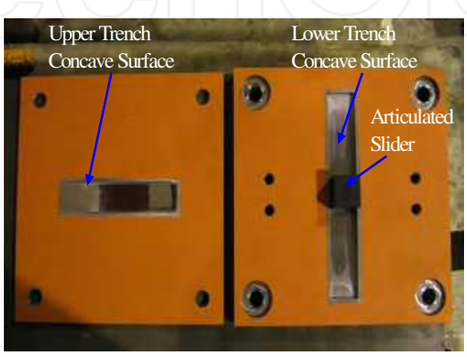

Fig. 9(a). Open-up view of trench friction pendulum system

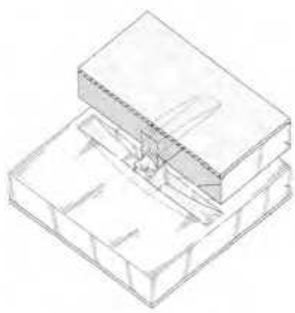

Fig. 9(b). A perspective view of trench friction pendulum system

In order to further enhance the functionality of the TFPS isolator (Tsai et al., 2010c), a base isolation system named the multiple trench friction pendulum system (MTFPS) with numerous intermediate sliding plates was proposed by Tsai et al. (2010d). As shown in Figures 10(a) and 10(b), the MTFPS isolator has multiple concave sliding interfaces that are composed of several sliding surfaces in each of two orthogonal directions, and an articulated slider located among trench concave sliding surfaces. The MTFPS represents more than one trench friction pendulum system connected in series in each direction. The friction coefficient, displacement capacity, and radius of curvature of each trench concave sliding surfaces in each direction can be different. The natural period and damping effect for a MTFPS isolator with several sliding surfaces can change continually during earthquakes. Therefore, a large number of possibilities of combinations are available for engineering designs. Such options are dependent on the needs of engineering practicing.

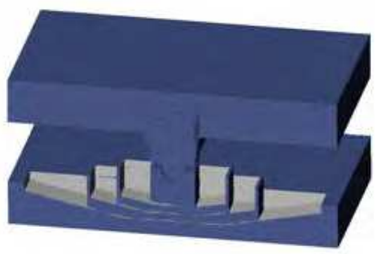

Fig. 10(a). Cross-sectional view of multiple trench friction pendulum system

Fig. 10(b). Perspective view of multiple trench friction pendulum system

As shown in Figs. 11(a) and 11(b), Tsai et al. (2007, 2008b) developed a direction-optimized friction pendulum system (DO-FPS) which consists of a spherical concave surface, a trench concave surface, as shown in Fig. 11(a), or a trajectory concave surface, as shown in Fig. 11(b), and an articulated slider. The DO-FPS isolator possesses important characteristics such as the natural period, displacement capacity and damping effect, which are functions of the directional angle of the sliding motion of the articulated slider during earthquakes. In order to improve the contact between the spherical and trench surfaces (or the trajectory concave surface), the slider consists of circular and square contact surfaces to match the spherical and trench surfaces, respectively. To further enhance the contact, it possesses a special articulation mechanism to accommodate any rotation in the isolator and maintain the stability of the isolated structures during earthquakes. In addition, the DO-FPS isolator can continually change the natural period and adjust the capacity of the bearing displacement and damping effect as a result of the change of the angle between the articulated slider and trench concave surface during earthquakes. This isolation system exhibits adaptive stiffness and adaptive damping by using different coefficients of friction and radii of curvature on the spherical and trench (or the trajectory) concave sliding surfaces to change the stiffness and damping to predictable values at specified and controllable angle of the sliding motion of the slider in the isolator although it is a completely passive device.

Fig. 11(a). Open-up view of first type direction optimized-friction pendulum system

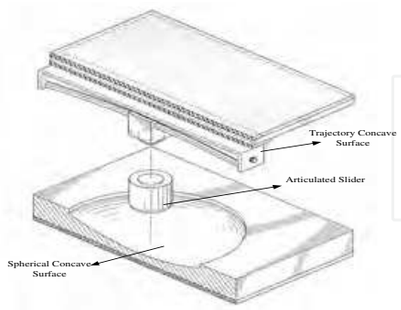

Fig. 11(b). Open-up view of second type direction optimized-friction pendulum system

As shown in Figures 12(a) and 12(b), Tsai et al. (2010e, 2011b) proposed and studied in theory and experiment on a base isolator that features variable natural period, damping effect and displacement capacity, named the multiple direction optimized-friction pendulum system (MDO-FPS). This device is mainly composed of several spherical concave sliding surfaces, several trench sliding concave surfaces and an articulated slider located

among these spherical and trench concave sliding surfaces to make the isolation period changeable with the sliding direction from only the multiple trench sliding interfaces to the combinations of the multiple trench sliding interfaces and the multiple spherical sliding interfaces.

In addition, this bearing may have *N* number of sliding interfaces in the trench and spherical surfaces to possess adaptive features of stiffness and damping by using different coefficients of friction and radii of curvature on the trench and spherical concave surfaces leading to changeable stiffness and damping at specified displacement amplitudes. Therefore, the MDO-FPS isolator possesses important characteristics in natural period, damping effect and displacement capacity, which are functions of the direction of the sliding motion, coefficients of friction and radii of curvature on sliding interfaces, and sliding displacements.

The advantage of the isolator is able to change its natural period, damping effect and displacement capacity continually during earthquakes to avoid possibility of resonance induced by ground motions. This base isolator has more important features and flexibility than other types of base isolation devices for engineering practice. Practicing engineers will be able to optimize the isolator at various levels of earthquakes by adopting suitable parameters of friction coefficients and radii of curvature of the sliding interfaces.

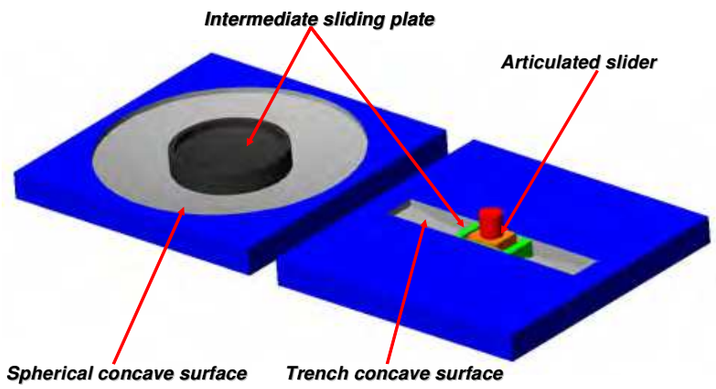

Fig. 12(a). Open-up view of MDO-FPS

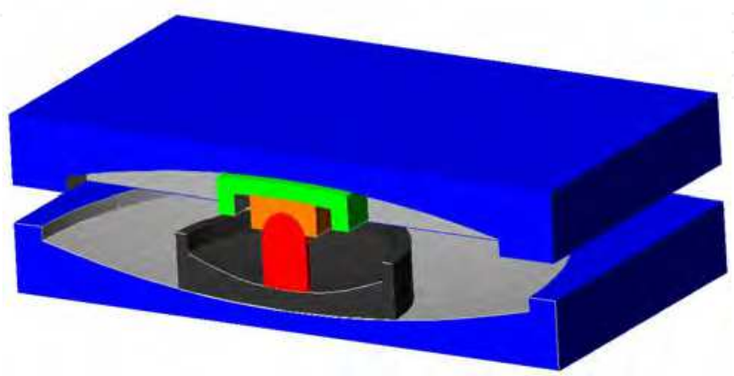

Fig. 12(b). Cross-sectional view of multiple direction optimized-friction pendulum system (MDO-FPS)

2. The static dynamics interchangeable – Ball pendulum system

The dynamics interchangeable–ball pendulum system (SDI-BPS) is schematized in Figs. 4(a) and 4(b) consisting of one upper concave surface (not necessary a spherical shape), one lower concave surface, several supporting steel balls to provide supports for long terms of service loadings and the frictional damping effect to the isolator at small displacements (see Case 1 of Fig. 13), several housing holes to lodge the supporting steel balls and one damped steel ball covered by damping materials to uphold the vertical loads resulting from the static and seismic loadings at large displacements (see Case 3 of Fig. 13) and supply additional damping to the bearing by deforming the damping material that could be a rubber material during earthquakes.

As shown in Case 1 of Fig. 13, almost all static loadings as a result of the weight of the equipment are sustained by the supporting steel balls and negligible loadings are taken by the damped steel ball while the system is under long terms of service loadings.

In the event of an earthquake, the static loadings and the dynamic loadings induced by the ground or floor accelerations are still supported by the supporting steel balls while the horizontally mobilized force is less than the total frictional force from the supporting steel balls, and the damped steel ball remains inactivated, similar to Case 1 of Fig. 13. The frictional force depends on the contact area and the coefficient of friction among the upper concave surface, the supporting steel balls and the housing holes located on the lower concave surface. This contact area and friction coefficient can be properly designed for the purpose of adjusting the frictional force and damping.

When the horizontal force exceeds the frictional force, the damped steel ball is activated and starts rolling on the concave surfaces. The vertical force resulting from the static and dynamic loadings is shared by the damped steel ball and the supporting steel balls. Simultaneously, the damping effect is provided by the supporting steel balls due to the frictional force and the damped steel ball as a result of the deformation of the damping material enveloping the damped steel ball under the condition of small isolator displacement, as shown in Case 2 of Fig. 13. The natural period of the isolated system is then dominated by the radii of curvature of the concave surfaces, which is equal to $2\pi\sqrt{\frac{R_1+R_2}{g}}$.

Where R_1 and R_2 are the radii of curvature of the upper and lower spherical concave surfaces, respectively; and g is the gravity constant.

If the system is subjected to a large isolator displacement during an earthquake, the supporting steel balls will be detached from the upper concave surface, and the total vertical and horizontal loads will be supported by the damped steel ball only to result in more damping effect due to the larger deformation of the damping material, and no damping effect results from the frictional force caused by the supporting steel balls, as depicted in Case 3 of Fig. 13. Furthermore, the natural period of the isolated equipment is governed by the radii of curvature of the concave surfaces in this stage. The damping effect for the isolator is only provided by the deformation of the damping material covering the damped steel ball in the course of motions to reduce the size of the isolator as a result of smaller isolator displacements caused by earthquakes in comparison to a rolling isolation system with negligible damping.

As shown in Case 4 of Fig. 13, because the component of the gravity force from the equipment weight tangential to the concave surface provides the restoring force, the

isolator will be rolling back to the original position without a significant residual displacement after earthquakes. Therefore, the damped steel ball is subjected to temporary loadings induced by earthquakes only, and the static loadings in the life span of service won't cause any permanent deformation to the damping material enveloping the damped steel ball.

In general, in the case of a service loading or a small earthquake, the static load is supported by the mechanism composed of the upper and lower concave surfaces and supporting steel balls with negligible supporting effect from the damped steel ball. On the other hand, in the events of medium and large earthquakes, the entire loads including static and dynamic loads are supported by the mechanism offered by the upper and lower concave surfaces and the damped steel ball while the isolation system is activated. These two mechanisms are interchangeable between the cases of static loading from the weight of equipment and seismic loading from the ground or floor acceleration.

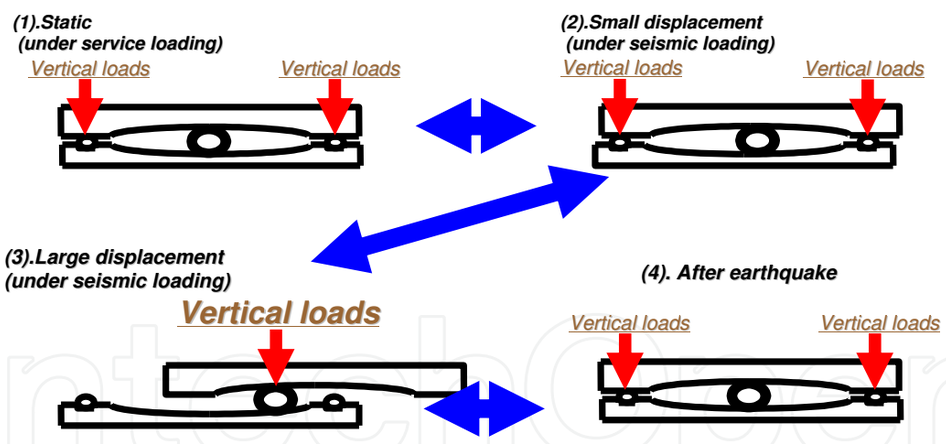

Fig. 13. Movements of a SDI-BPS isolator under service and seismic loadings

2.1 Characteristic of the SDI-BPS isolator

The test setup of the SDI-BPS isolator is depicted in Figures 14(a) and 14(b). In this test, the damped steel ball consisted of a steel rolling ball of 44.55mm in diameter covered with a thickness of 6.75mm damping material which was made of natural rubber material with hardness of 60 degrees in the IRHD standard (International Rubber Hardness Degree). The main purpose of this test was to investigate the mechanical behavior of the damped steel ball, therefore, supporting balls were removed during the component tests and all damping effect resulting from the system was provided by the damped steel ball. Figure 15 shows the relationship of the horizontal force to the horizontal displacement while the system was subjected to a vertical load of 4.56 *KN* and a harmonic displacement of 50mm with a frequency of 0.3Hz. The enclosed area shown in the Fig. 15 provides a damping effect into the isolation system. The test result demonstrates that the deformations of the rubber material leaded to significant damping effects in the system with negligible deformation occurring in the steel material.

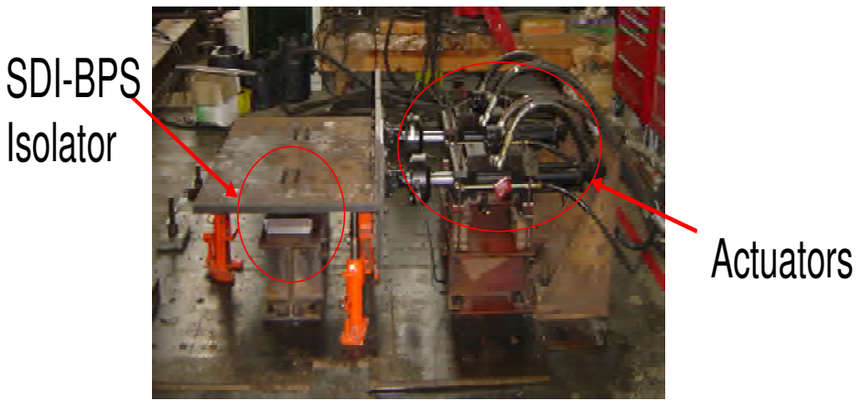

Fig. 14(a). Setup for component tests of the SDI-BPS isolator

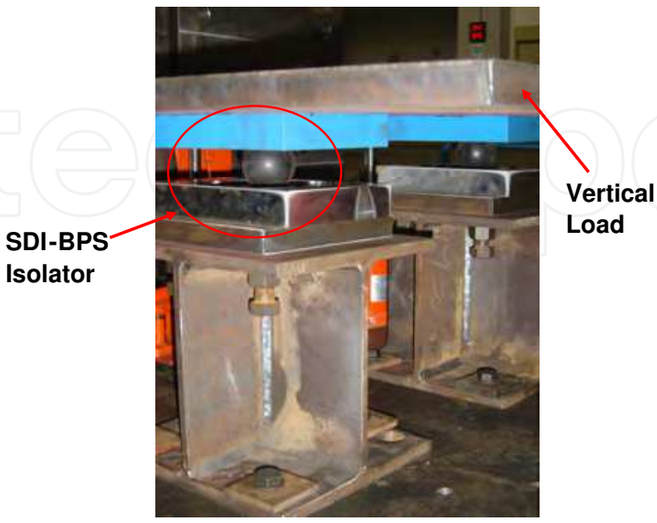

Fig. 14(b). Close view of component test of SDI-BPS isolator

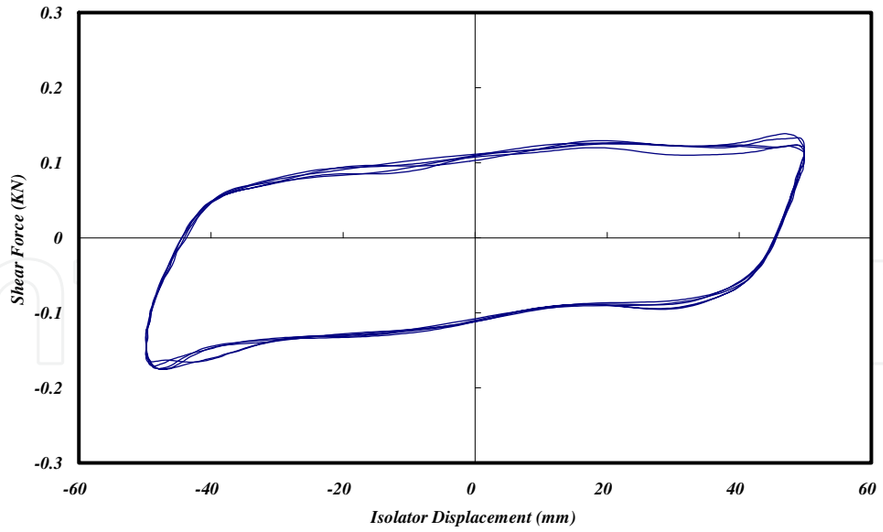

Fig. 15. Hysteresis loop of SDI-BPS isolator without supporting balls

2.2 Shaking table tests of motion sensitive equipment with SDI-BPS isolators

This section will investigate the performance of the SDI-BPS isolator installed in the motion sensitive equipment on seismic mitigation under tri-directional earthquakes through a series of shaking table tests of the vibration sensitive equipment isolated with the SDI-BPS isolator under tri-directional earthquakes. As shown in Figure 16, the tested vibration sensitive equipment with six inner layers was used to house the network server. The lengths in the two horizontal directions were 0.8 m and 0.6 m, respectively, and 1.98 m in height. The mass of the empty equipment was 110 kg. A mass of 108 kg at each layer from the first to the third layer and 54 kg each at the rest of the layers was added. In the case of the fixed base equipment, the natural frequency was 5.66 Hz. In the case of the isolated system, four SDI-BPS isolators with a radius of curvature of 1.0 m representing 2.84 seconds in natural period for the isolated equipment were installed beneath the equipment.

The input ground motions in these tests included the 1995 Kobe earthquake (Japan) and the 1999 Chi-Chi earthquake (recorded at TCU084 station, Taiwan). Figures 17(a) and 17(b) show the comparisons of the acceleration responses at the top layer of the equipment between the fixed base and SDI-BPS-isolated systems under tri-directional earthquakes. It is observed from these figures that the SDI-BPS isolator can effectively isolate the seismic energy trying to transmit into the vibration sensitive equipment during earthquakes. Figures 18(a) and 18(b) show the hysteresis loops of the SDI-BPS isolator under the various tri-directional earthquakes. These figures illustrate that the SDI-BPS isolator can provide damping to limit the bearing displacement, and accordingly, the bearing size was decreased. It also infers from these figures that a frictional type of damping was provided by the isolation system in small displacements and other type of damping was provided by the damped steel ball of the isolation system for large displacements, referring to the hysteresis loop in Figure 15, because the upper concave surface was lifted and away from the supporting steel balls without any contact. The isolator displacement history depicted in Figure 19 demonstrates that the response of equipment had been reduced by the isolation system with acceptable displacements in the isolators and that the isolator displacement approached zero in the end of the earthquake with negligible residual displacement.

Fig. 16. Vibration sensitive equipment isolated with SDI-BPS isolators

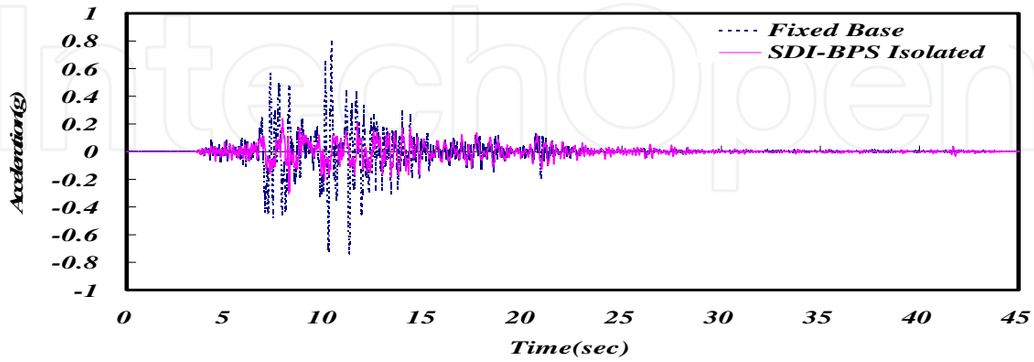

Fig. 17(a). Comparison of X-directional acceleration response at top layer between fixed-base and SDI-BPS-isolated systems under tri-directional Kobe earthquake (PGA = X0.388g + Y0.265g + Z0.116g)

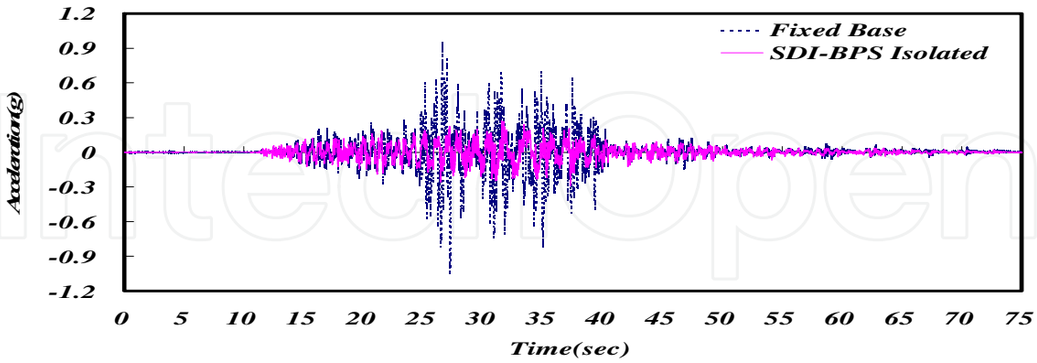

Fig. 17(b). Comparison of acceleration response in X-direction at top layer between fixed-base and SDI-BPS-isolated systems under tri-directional Chi-Chi (TCU084 Station) earthquake (PGA = X0.673g + Y0.271g + Z0.159g)

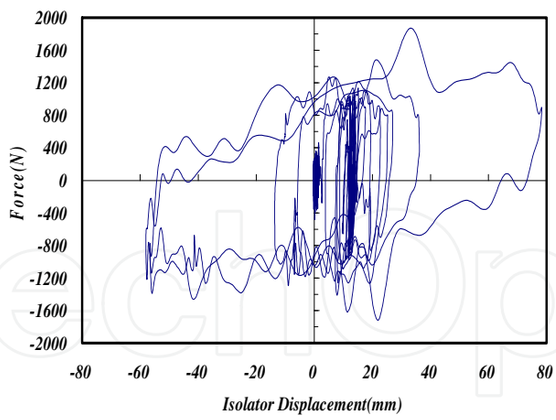

Fig. 18(a). Hysteresis loops of SDI-BPS isolator in X direction under tri-directional Kobe earthquake (PGA = X0.388g + Y0.265g + Z0.116g)

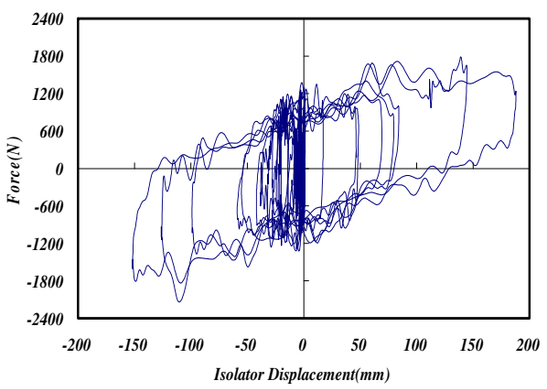

Fig. 18(b). Hysteresis loops of SDI-BPS isolator in X direction under tri-directional Chi-Chi (TCU084 Station) earthquake (PGA = X0.673g + Y0.271g + Z0.159g)

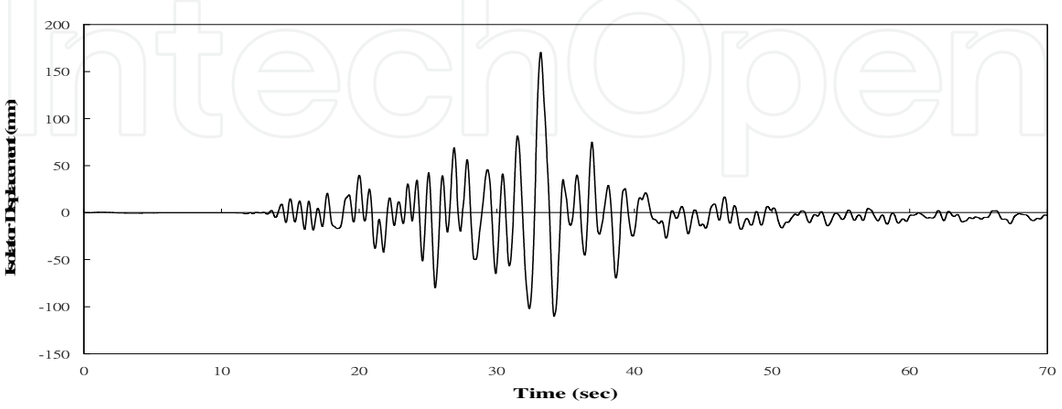

Fig. 19. Isolator displacement history in X-direction while isolated system subjected to tri-directional Chi-Chi (TCU084 Station) earthquake (PGA = X0.513g + Y0.170g +Z0.151g)

3. The direction-optimized friction pendulum system

A seismic isolation system, called the direction-optimized friction pendulum system (DO-FPS), consists of a concave trench, a plate with a spherically concave surface, and an articulated slider located in between, as shown in Figs. 20(a) and 20(b). The trench and the plate can usually possess different curvature radii, friction coefficients, and displacement capacities. As shown in Fig. 20(b), the concave trench is connected in series with the spherically concave plate in the X-direction, and this provides both the maximum natural period and the maximum displacement capacity. By contrast, in the Y-direction the isolator consists of just the spherically concave plate, and this provides both the minimum natural period and the minimum displacement capacity. The natural period and the displacement capacity vary with direction and are functions of the sliding angle between the articulated slider and the concave trench. In engineering practice, the DO-FPS isolator can be designed for differences in natural period and displacement capacity for the purpose of cost-effectiveness. During an earthquake, the DO-FPS isolator will adjust the natural period automatically to avoid the possibility of resonance. Following the earthquake, the concave trench and the spherically concave plate can offer a centering mechanism to return the isolated structure to its original position without significant residual displacements.

Fig. 20(a). Assembly of direction optimized friction pendulum system

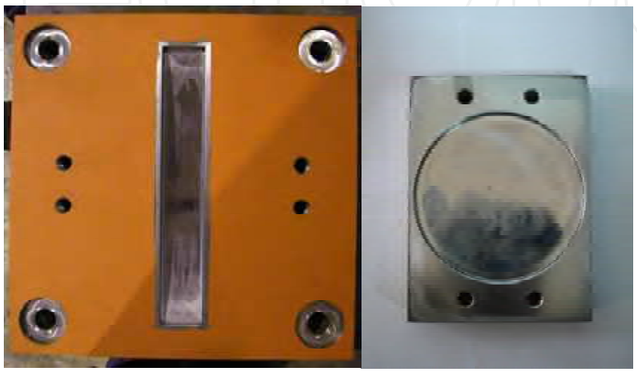

Fig. 20(b). An open-up view of the DO-FPS isolator with trench and concave surface

3.1 Properties of the direction-optimized friction pendulum system

As shown in Figs. 21(a) and 21(b), an articulated slider is located between the concave trench and the spherically concave plate. The articulated slider includes two parts: the lower part at the trench side can have a rectangular cross section, while the upper part at the plate side can have a circular cross section. These two parts are joined with a hemispherical joint to produce an articulation mechanism in the middle of the slider. Hence, the articulated slider incorporates a rotational function to accommodate the relative rotation during its movement. As shown in Fig. 21(a), the slider is coated with Teflon composite on top, bottom, and two sides to reduce the frictional forces at its interfaces with not only the concave surfaces of the trench and plate but also the side walls of the trench.

Fig. 21(a). Assembly of articulated slider coated with Teflon composite

Fig. 21(b). Slider located between the concave trench and the spherical concave surface.

As shown in Fig. 21(b), the width of the articulated slider almost equals that of the trench; therefore, the sides of the slider and the walls of the trench almost remain in contact. These two sides of the articulated slider can thus provide additional damping in the direction parallel to the concave trench to help dissipate seismic energy.

3.2 Component tests of sliding interfaces

Figures 22(a) and 22(b) respectively show the schematic design and the test setup for the Teflon composite coated on the sliding surfaces. To examine the sliding characteristic of the sliding surface, the steel plates were coated with the Teflon composite and the high density chrome, respectively, to rub against each other. During the tests, the vertical pressures imposing at the interface are variable values.

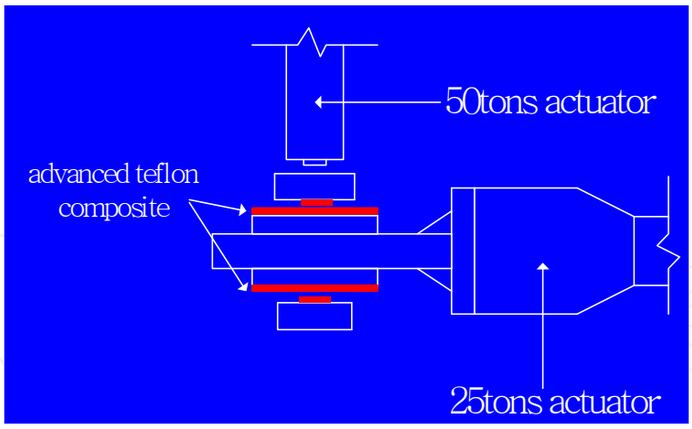

Fig. 22(a). The schematic design for the test of the Teflon composite

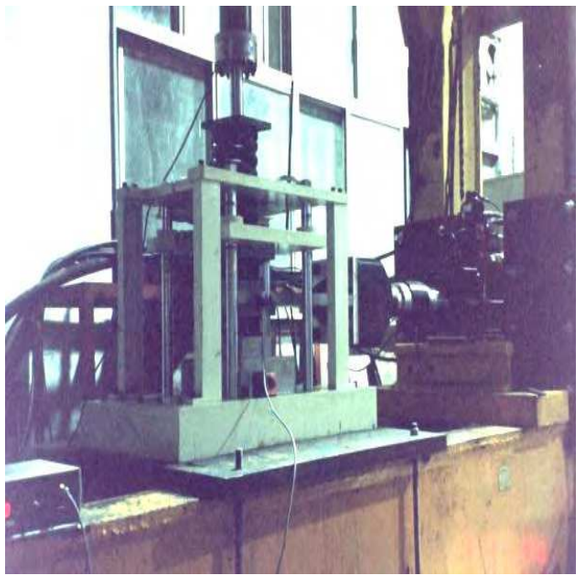

Fig. 22(b). Test setup for the Teflon composite

Figure 23 depicts a typically hysteretic loop when the vertical pressure was 98Mpa. Figure 24 demonstrate that the coefficients of friction are functions of the vertical pressure on the contact surface and the velocity of the sliding motion. In accordance with the analytical model proposed by Tsai (2005a), the total friction force acting on the sliding interface can be expressed as:

$$\mu(\dot{u}_b) = \frac{A}{\lambda_1 A + \lambda_2 P} \cdot \{1 + \alpha[1 - \exp(-\beta|\dot{u}_b|)]\} \times Coef \tag{2}$$

where A represents the contact area at the sliding interface; λ_1 and λ_2 denote the parameters associated with the quasi-static friction force at the zero velocity; P is the contact force normal to the sliding surface; and α is the amplification factor used to describe the increase of friction force with increasing the sliding velocity; and β is the parameter which controls the variation of the friction coefficient with sliding velocity; and $\dot{u}_b$ is the siding velocity of the base isolator.

The term $A/\lambda_1 A + \lambda_2 P$ is used to describe the friction coefficient at zero velocity. According to the experimental observations, the friction coefficient depends on the sliding velocity. Therefore, the term $1+\alpha\left[1-\exp(-\beta|\dot{u}_b|)\right]$ is used to describe the amplification factor of the friction coefficient relative to that at zero velocity. The coefficient, *Coef* , is a decay function representing the phenomenon of degradation of the friction force with the increase of the number of cyclic reversals. The coefficient of *Coef* can be shown as:

$$Coef = (1-\gamma_1) + \gamma_1 \cdot \exp(-\gamma_2 \cdot \int_0^t \frac{F_t - F_t^0}{F_t^0} \cdot du_b) \tag{3}$$

where γ_1 and γ_2 are parameters to describe the decay behavior of the friction coefficient at the Teflon interface associated with the energy accumulation in the history of the sliding motion; F_t^0 is the friction force when the sliding velocity is equal to zero; F_t is the friction force at current time *t;* and du_b is the displacement increment of the base isolator. The effect of the coefficient, *Coef,* may be neglected for the purpose of engineering practice.

$$\lambda_1 = 21.120 \quad , \quad \lambda_2 = 1.221\times10^{-7}(1/Pa)$$

$$\alpha = 1.903 \quad , \quad \beta = 100.000(\sec/m)$$

$$\gamma_1 = 0.1390 \quad , \quad \gamma_2 = 7.1537(1/m)$$

According to the model proposed by Al-Hussaini et al. (1994), the friction coefficient can be represented in the following form:

$$\mu(\dot{u}_b) = \mu_{\max} - (\mu_{\max} - \mu_{\min})\exp(-\beta|\dot{u}_b|) \tag{4}$$

where $\mu_{\min}$ and $\mu_{\max}$ are the friction coefficients at zero sliding velocity and high sliding velocity, respectively.

Figure 25 shows the comparison between the theoretical and experimental results. It can be concluded that the numerical result obtained from the mathematical model has good agreement with the experimental results.

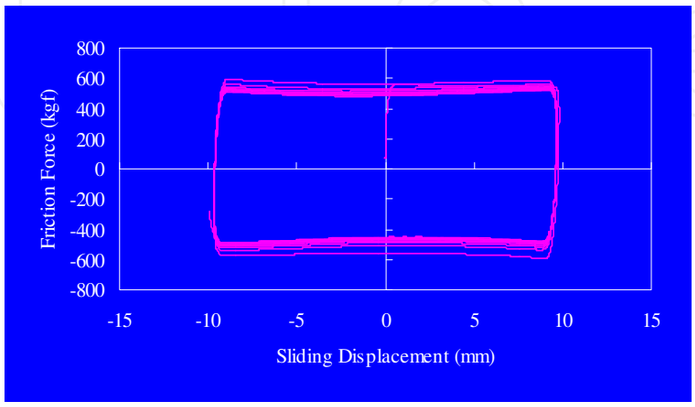

Fig. 23. Typical hysteretic loop for the Teflon composite under a vertical pressure of 98 Mpa and a Frequency of 1Hz

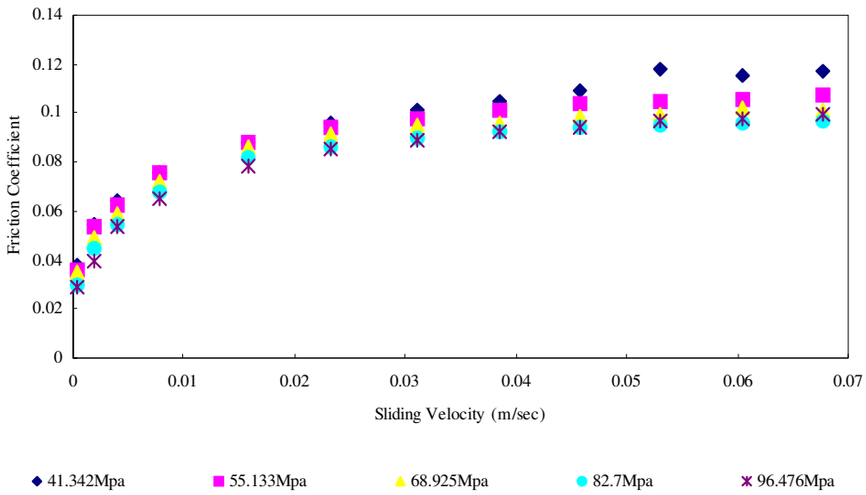

Fig. 24. Friction coefficients under various vertical pressures

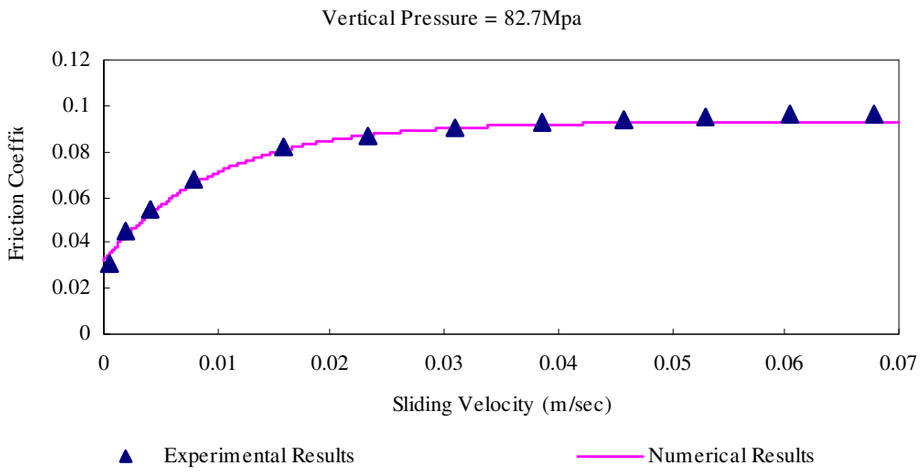

Fig. 25. Friction coefficients under various sliding velocities

3.3 Equation of motion for a rigid mass isolated with DO-FPS isolators

As shown in Fig. 26, the time history of ground accelerations can be represented by the method of interpolation of excitation by assuming that the ground motion is a linear variation between time t_{i-1} and t_i. If a rigid mass is isolated with DO-FPS isolators, as shown in Fig. 27, the equation of motion can be expressed as:

$$m\ddot{u}_b + c_b\dot{u}_b + k_b u_b = -\mu(\dot{u}_b)mg\,\mathrm{sgn}(\dot{u}_b) - m\ddot{u}_g^{i-1} - \frac{m\ddot{u}_g^{i} - m\ddot{u}_g^{i-1}}{\Delta t}\tau \tag{5}$$

where m, c_b and k_b are the mass, damping coefficient and horizontal stiffness of the isolated mass, respectively; u_b is the displacement of the base isolator relative to the ground; $\mu(\dot{u}_b)$ is the friction coefficient of the sliding surface, which is a function of sliding velocity; and $\ddot{u}_g^i$ is the ground acceleration at time t_i.

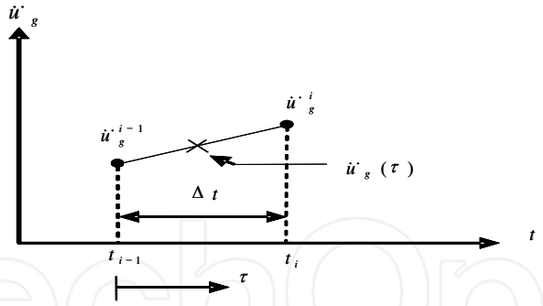

Fig. 26. Linear Interpolation for Ground Motions

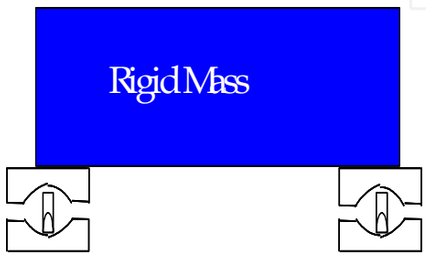

Fig. 27. A rigid mass isolated with DO-FPS isolator

The transient response of Eq. (5) can be given by:

$$u_c(\tau) = (A\cos\omega_d\tau + B\sin\omega_d\tau)\exp(-\xi\omega_n\tau) \tag{6}$$

where ω_n is the natural frequency; $\omega_d = \omega_n\sqrt{1-\xi^2}$ is the damped frequency; ξ is the viscous damping ratio.

The particular solution of Eq. (5) between time t_{i-1} and t_i can be given by:

$$u_p(\tau) = \frac{1}{\omega_n^2}\left[-\mu(\dot{u}_b)g\,\mathrm{sgn}(\dot{u}_b) - \ddot{u}_g^{i-1} + \frac{2\xi}{\omega_n\Delta t}(\ddot{u}_g^{i} - \ddot{u}_g^{i-1})\right] - \frac{\ddot{u}_g^{i} - \ddot{u}_g^{i-1}}{\omega_n^2\Delta t}\tau \tag{7}$$

The sliding displacement of the base isolator between time t_{i-1} and t_i can be obtained from Eqs. (6) and (7) as:

$$\begin{aligned} u_b(\tau) &= (A\cos\omega_d\tau + B\sin\omega_d\tau)\exp(-\xi\omega_n\tau) \\ &+ \frac{1}{\omega_n^2}\left[-\mu(\dot{u}_b)g\,\mathrm{sgn}(\dot{u}_b) - \ddot{u}_g^{i-1} + \frac{2\xi}{\omega_n\Delta t}(\ddot{u}_g^{i} - \ddot{u}_g^{i-1})\right] - \frac{\ddot{u}_g^{i} - \ddot{u}_g^{i-1}}{\omega_n^2\Delta t}\tau \end{aligned} \tag{8}$$

At the beginning of each time step, the sliding displacement is equal to that at the end of the previous time step, i.e. $u_b(0) = u_b^{i-1}$.

The coefficient *A* of Equation (6) can be obtained as:

$$A = u_b^{i-1} - \frac{1}{\omega_n^2}\left[-\mu(\dot{u}_b)g\,\mathrm{sgn}(\dot{u}_b) - \ddot{u}_g^{i-1} + \frac{2\xi}{\omega_n\Delta t}(\ddot{u}_g^{i} - \ddot{u}_g^{i-1})\right] \tag{9}$$

The derivative of Eq. (8) respect to τ leads to:

$$\begin{aligned}\dot{u}_b(\tau) &= (-\omega_d A\sin\omega_d\tau + \omega_d B\cos\omega_d\tau)\exp(-\xi\omega_n\tau)\\ &-\xi\omega_n(A\cos\omega_d\tau + B\sin\omega_d\tau)\exp(-\xi\omega_n\tau) - \frac{\ddot{u}_g^i - \ddot{u}_g^{i-1}}{\omega_n^2\Delta t}\end{aligned} \tag{10}$$

Backsubstitution of $\dot{u}_b(0) = \dot{u}_b^{i-1}$ into Eq. (10) results in:

$$B = \frac{1}{\omega_d}(\dot{u}_b^{i-1} + \xi\omega_n A + \frac{\ddot{u}_g^i - \ddot{u}_g^{i-1}}{\omega_n^2\Delta t}) \tag{11}$$

The sliding acceleration of the base isolator relative to the ground can be given by:

$$\begin{aligned}\ddot{u}_b(\tau) &= (-\omega_d^2 A\cos\omega_d\tau - \omega_d^2 B\sin\omega_d\tau)\exp(-\xi\omega_n\tau)\\ &-2\xi\omega_n(-\omega_d A\sin\omega_d\tau + \omega_d B\cos\omega_d\tau)\exp(-\xi\omega_n\tau)\\ &+\xi^2\omega_n^2(A\cos\omega_d\tau + B\sin\omega_d\tau)\exp(-\xi\omega_n\tau)\end{aligned} \tag{12}$$

3.3.1 Condition for non-sliding phase

The kinetic friction coefficient has been considered as the same as the static friction coefficient. Therefore, as the summation of the inertia and restoring forces imposing at the base raft is lower than the quasi-static friction force, i. e.:

$$\left|m(\ddot{u}_b + \ddot{u}_g) + c_b\dot{u}_b + k_b u_b\right| < \mu_{\min} mg \tag{13}$$

Then the structure will behave as a conventional fixed base structure, and the sliding displacement, sliding velocity and relative acceleration are:

$$u_b = \text{constant}\,,\ \dot{u}_b = \ddot{u}_b = 0 \tag{14}$$

3.3.2 Initiation of sliding phase

The base isolated rigid mass will behave as a fixed base structure unless the static friction force can be overcome. During the sliding phase, the equation given in the following should be satisfied:

$$\left|m(\ddot{u}_b + \ddot{u}_g) + c_b\dot{u}_b + k_b u_b\right| \geq \mu_{\min} mg \tag{15}$$

Because the time increment adopted in the time history analysis (e.g. $\Delta t = 0.0005\,\text{sec}$) is quite smaller than that of the sampling time of the earthquake history, it is reasonable to assume that the direction of sliding at the current time step is the same as the previous time step. It should be noted that the direction of sliding remains unchanged during a particular sliding phase. At the end of each time step, the validity of inequality Eq. (15) should be checked. If the inequality is not satisfied at a particular time step, then the structure enter a non-sliding phase and behaves as a fixed base structure.

3.3.3 Simplified mathematical model for DO-FPS isolator

The simplified model based on the equilibrium at the slider of the DO-FPS isolator can be shown in the following. As shown in Fig. 28, horizontal forces F_1 and F_2 imposing at the concave trench and spherical sliding surfaces, respectively, can be expressed as:

$$F_1 = \frac{W}{R_1} u_1 + \mu W \operatorname{sgn}(\dot{u}_1) \tag{16}$$

and

$$F_2 = \frac{W}{R_2} u_2 + \mu W \operatorname{sgn}(\dot{u}_2) \tag{17}$$

where W is the vertical load resulting from the superstructure ; R_1 and R_2 represent the radii of curvature of the concave trench and spherical sliding surfaces, respectively; u_1 and u_2 depict the horizontal sliding displacements of the slider relative to the centers of the concave trench and spherical sliding surfaces, respectively; μ represents the friction coefficient for the Teflon composite interface which depends on the sliding velocity; and $\dot{u}_1$ and $\dot{u}_2$ are the sliding velocities of the articulated slider.
Rearrangement of Eqs. (16) and (17) leads to:

$$u_1 = \frac{F_1 - \mu W \operatorname{sgn}(\dot{u}_1)}{W / R_1} \tag{18}$$

and

$$u_2 = \frac{F_2 - \mu W \operatorname{sgn}(\dot{u}_2)}{W / R_2} \tag{19}$$

With the aid of equilibrium at the articulated slider ($F = F_1 = F_2$), the total relative displacement between the centers of the concave trench and spherical sliding surfaces can be obtained as:

$$u_b = u_1 + u_2 = \frac{F - \mu W \operatorname{sgn}(\dot{u}_1)}{W / R_1} + \frac{F - \mu W \operatorname{sgn}(\dot{u}_2)}{W / R_2} \tag{20}$$

Rearrangement of Eq. (20) results in the base shear force:

$$F = \frac{W}{R_1 + R_2} u_b + \frac{R_1 \mu W \operatorname{sgn}(\dot{u}_1) + R_2 \mu W \operatorname{sgn}(\dot{u}_2)}{R_1 + R_2}_{f} = K_b u_b + F_f \tag{21}$$

where K_b represents the horizontal stiffness of the DO-FPS isolator and can be expressed as:

$$K_b = \frac{W}{R_1 + R_2} \tag{22}$$

Hence, the isolation period of the DO-FPS isolated structure in the direction of the concave trench surface is as follows:

$$T_b = 2\pi\sqrt{\frac{m}{k_b}} = 2\pi\sqrt{\frac{R_1 + R_2}{g}} \tag{23}$$

Based on the exact solution, the relationship between the base shear force and sliding displacement can be obtained by using Eqs. (21) and (8).

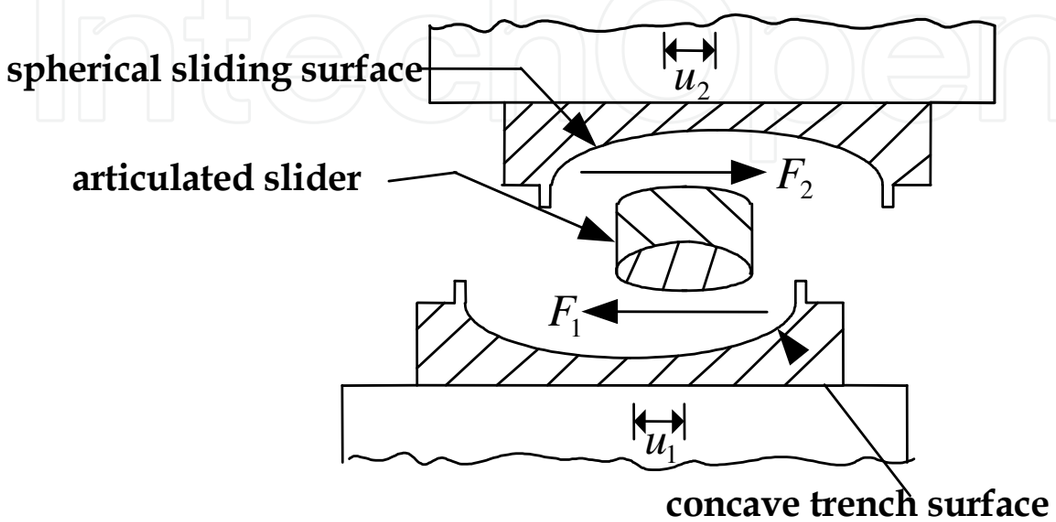

Fig. 28. The equilibrium of the forces on the spherical sliding and concave trench surfaces

3.3.4 Comparison of experimental and analytical results

In order to verify the accuracy of the exact solution derived in the previous sections, the shaking table tests of a rigid mass isolated with DO-FPS isolators were performed in Taiwan. The strong ground motions of the 1999 Chi-Chi (TCU084) have been given as earthquake loads during the shaking table tests. The DO-FPS isolator adopted in the shaking table tests has a concave trench and spherical sliding surfaces of 2.236m in radius of curvature. The fundamental period of the base isolated structure in the trench direction is 4.242sec.

The comparisons of the bearing displacement and velocity histories between the experimental and analytical results under the 1999 Chi-Chi earthquake (TCU084, EW component) of 1.211g in PGA are shown in Figs. 29(a) and 29(b), respectively. These figures tell us that the proposed solution can well simulate the sliding displacement and velocity of the nonlinear behavior of the device under strong ground motions. Figures 30(a) and 30(b) display the comparison between the recorded force-displacement loop and the calculated results for the DO-FPS base isolator. The results obtained from the numerical analysis are quite consistent with those from the experiments. The proposed algorithm can be given as a good tool for engineering professions to preliminarily design the displacement capacity and isolation period, etc. It should be noted that the method for the numerical analysis proposed in the previous section is only suitable for unidirectional loadings.

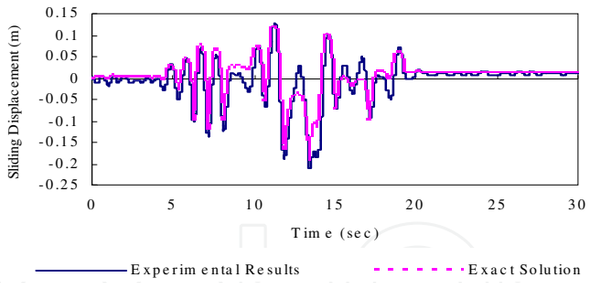

Fig. 29(a). Comparison of sliding displacement of DO-FPS isolator during 1999 Chi-Chi earthquake (TCU084, EW Component) of 1.211g in PGA

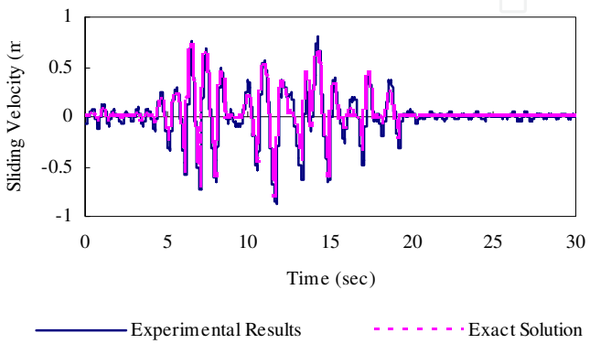

Fig. 29(b). Comparison of bearing sliding velocity between experimental and numerical results under 1999 Chi-Chi earthquake (TCU084, EW Component) of 1.211g in PGA

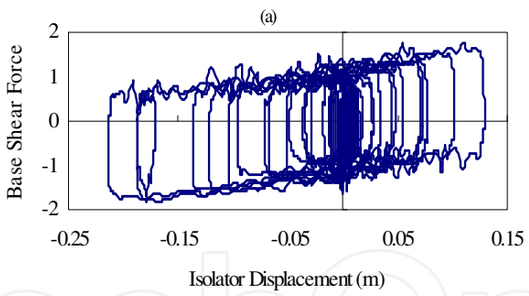

Fig. 30(a). Hysteresis loop of DO-FPS isolator under 1999 Chi-Chi earthquake (TCU084, EW Component) of 1.211g in PGA: (a) Experimental Results

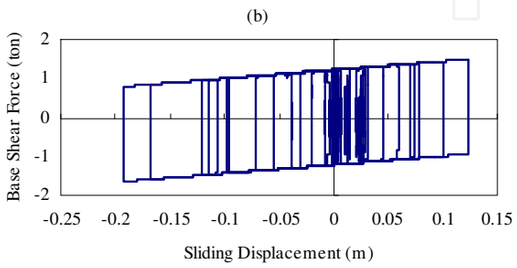

Fig. 30(b). Hysteresis loop of DO-FPS isolator under 1999 Chi-Chi earthquake (TCU084, EW Component) of 1.211g in PGA: (b) Exact Solution

3.4 Shaking table tests of equipment isolated with DO-FPS isolators

In order to examine the seismic behavior of motion sensitive equipment isolated with a direction-optimized friction pendulum system, a series of shaking table tests were carried out in the Department of Civil Engineering at Feng Chia University, as shown Fig. 31. In this full-scale experiment, a modem rack was adopted to simulate high-technology equipment such as server computers and workstations. The dimensions of the critical equipment were 0.8 m × 0.6 m × 1.98 m (length × width × height). Within the critical equipment were six levels, and lumped masses in the range from 50 kg to 100 kg were placed on these in 10 kg increments from top to bottom. The fundamental period of the critical equipment without isolators was measured in the shaking table test as 0.18 s.

In order to prove the benefit provided by the DO-FPS isolator, we used two extreme conditions with angles of 0° and 90°, respectively. The input ground motions included those of the earthquakes at El Centro (USA, 1940), Kobe (Japan, 1995), and Chi-Chi (station TCU084, Taiwan, 1999). Accelerometers and LVDTs were installed to measure the accelerations and displacements of the critical equipment plus DO-FPS isolators when subjected to the various ground motions.

Fig. 31. Critical equipment isolated with DO-FPS isolators

Figures 32(a) and 32(b) show comparisons of the roof acceleration responses of the critical equipment with and without DO-FPS isolators for angles of 0° and 90°, respectively, under the conditions of the El Centro earthquake (PGA of 0.4g). Figures 33(a) and 33(b) show analogous comparisons for the Kobe earthquake (PGA of 0.35g), while Figures 34(a) and 34(b) show those for the Chi-Chi earthquake (PGA of 0.3g). These results illustrate that the direction-optimized friction pendulum system effectively reduced the responses of the critical equipment by lengthening its fundamental period.

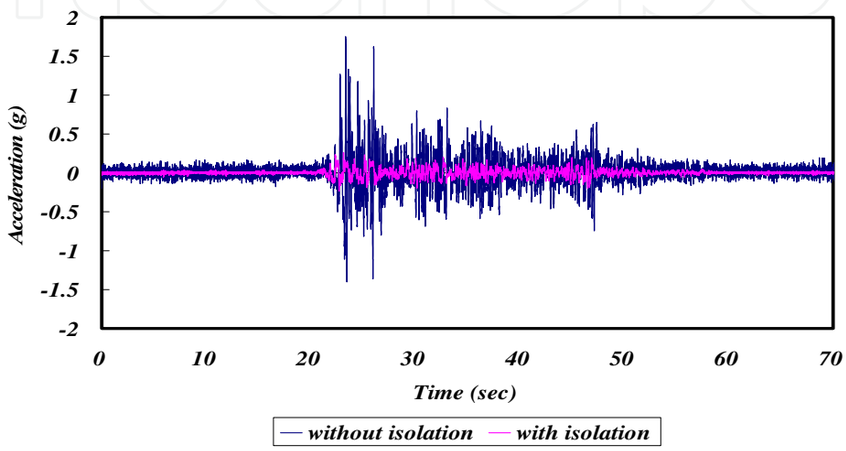

Fig. 32(a). Roof acceleration of equipment with and without DO-FPS isolators at angle of 90°under El Centro earthquake of 0.4g PGA

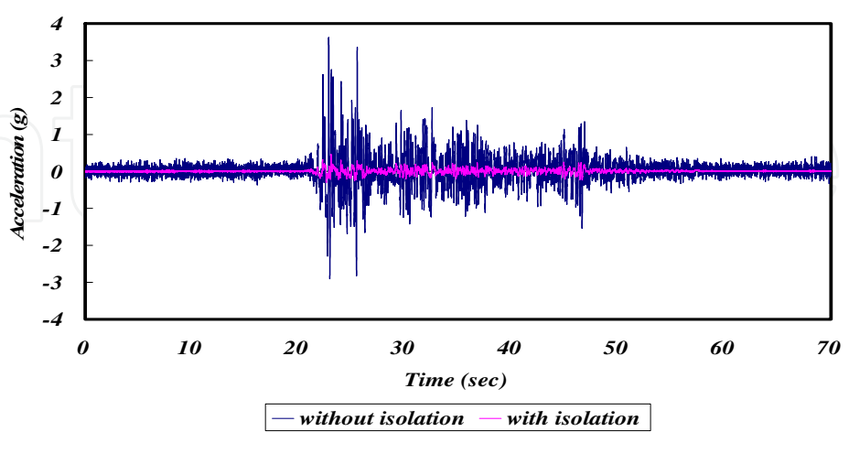

Fig. 32(b). Roof acceleration of equipment with and without DO-FPS isolators at angle of 0°under El Centro earthquake of 0.4g PGA

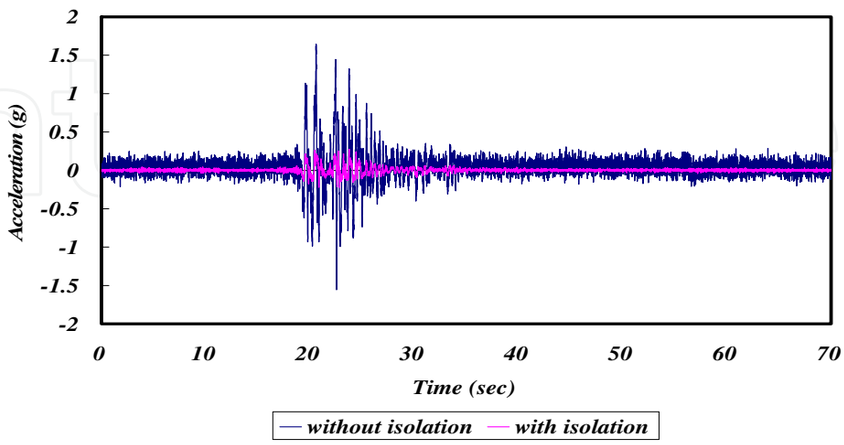

Fig. 33(a). Roof acceleration of equipment with and without DO-FPS isolators under at angle of 90° Kobe earthquake of 0.35g PGA

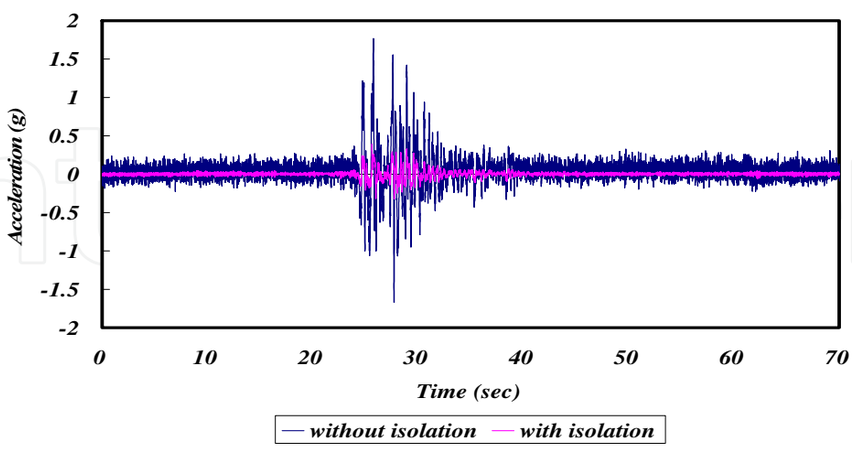

Fig. 33(b). Roof acceleration of equipment with and without DO-FPS isolators at angle of 0°under Kobe earthquake of 0.35g PGA

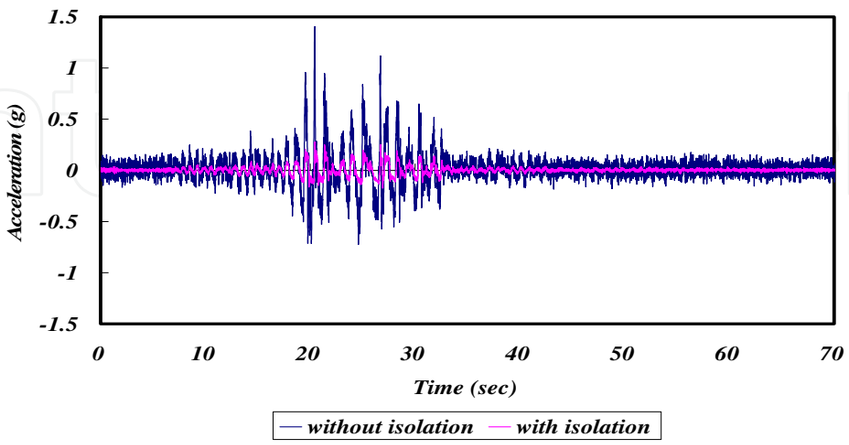

Fig. 34(a). Roof acceleration of equipment with and without DO-FPS isolators under at angle of 90° Chi-Chi earthquake of 0.3g PGA

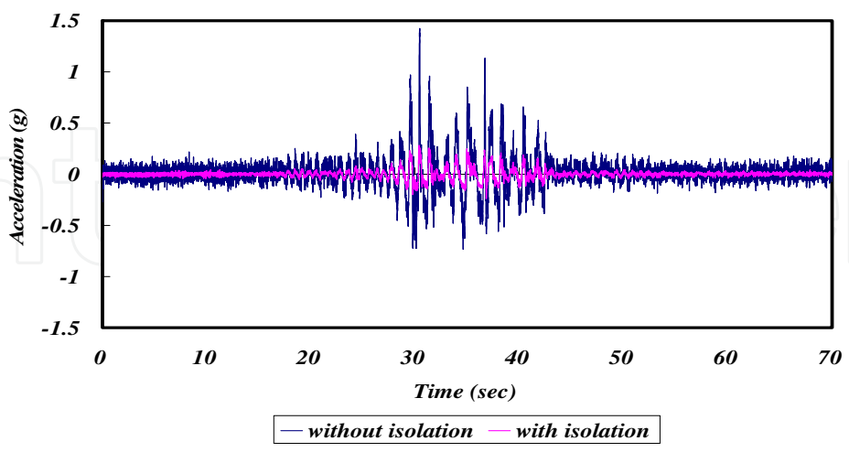

Fig. 34(b). Roof acceleration of equipment with and without DO-FPS isolators at angle of 0° under Chi-Chi earthquake of 0.3g PGA

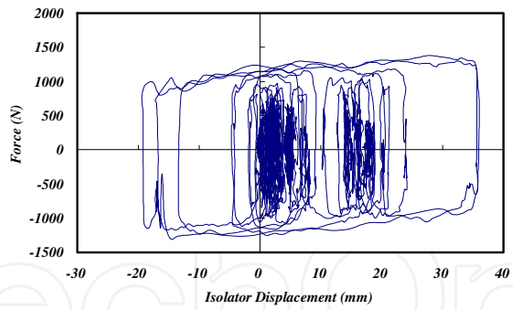

Fig. 35(a). Hysteresis loop of DO-FPS isolator at angle of 90° during 0.4 g El Centro ground motion

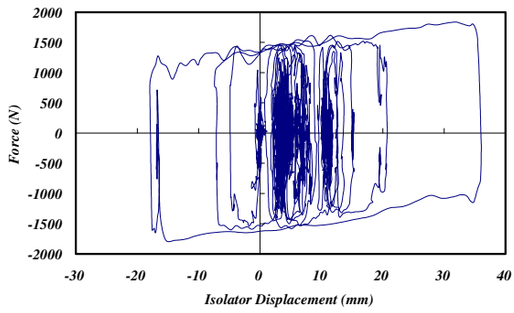

Fig. 35(b). Hysteresis loop of DO-FPS isolator at angle of 0° during 0.4 g El Centro ground motion

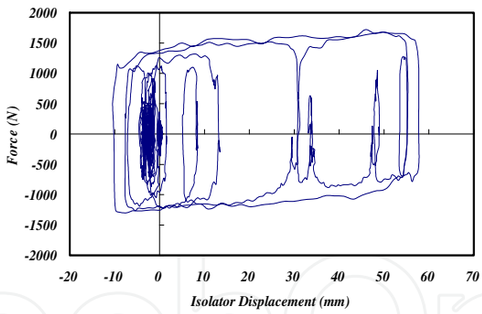

Fig. 36(a). Hysteresisloop of DOFPS isolator at angle of 90° during 0.35 g Kobe ground motion

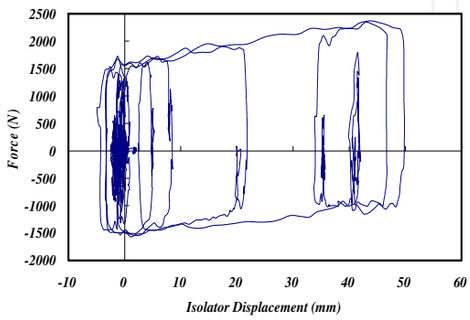

Fig. 36(b). Hysteresis loop of DO-FPS isolator at angle of 0° during 0.35 g Kobe ground motion

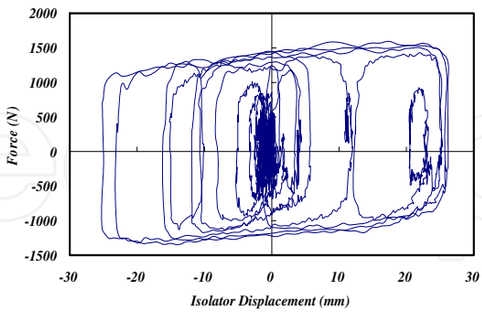

Fig. 37(a). Hysteresis loop of DOFPS isolator at angle of 90° during 0.3 g Chi-Chi ground motion

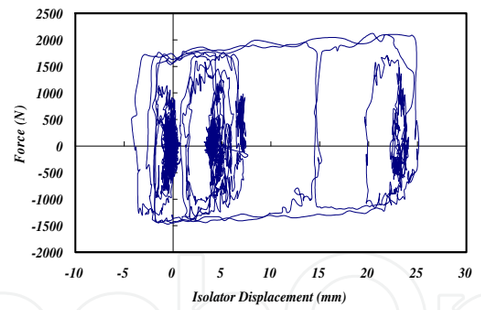

Fig. 37(b). Hysteresis loop of DOFPS isolator at angle of 0° during 0.3 g Chi-Chi ground motion

Figures 35(a) to 37(b) show the hysteresis loops of the DO-FPS isolator under the various earthquake conditions. The enclosed areas in these figures demonstrate that the DO-FPS isolator provided excellent damping of the entire system during the simulated earthquakes. Figures 38(a) to 40(b) show the roof displacement responses of the critical equipment. These figures illustrate that the DO-FPS isolator has a good mechanism for bringing the isolator back to its original position without significant displacements.

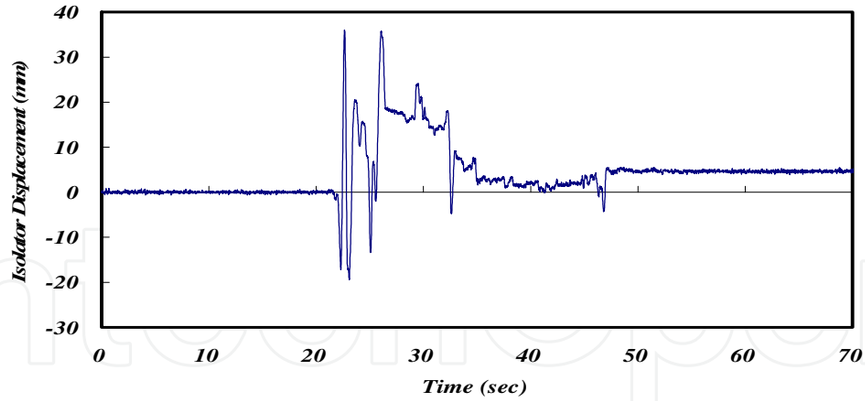

Fig. 38(a). Base isolator displacement of DOFPS isolator at angle of 90° during 0.4 g El Centro ground motion

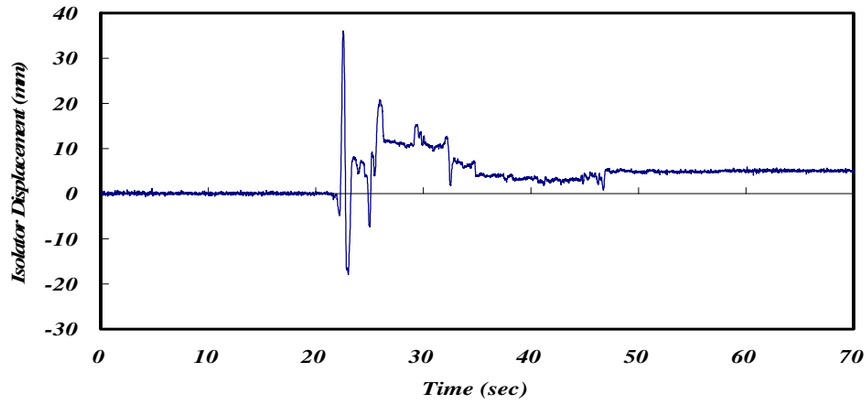

Fig. 38(b). Base isolator displacement of DO-FPS isolator at angle of 0° during 0.4 g El Centro ground motion

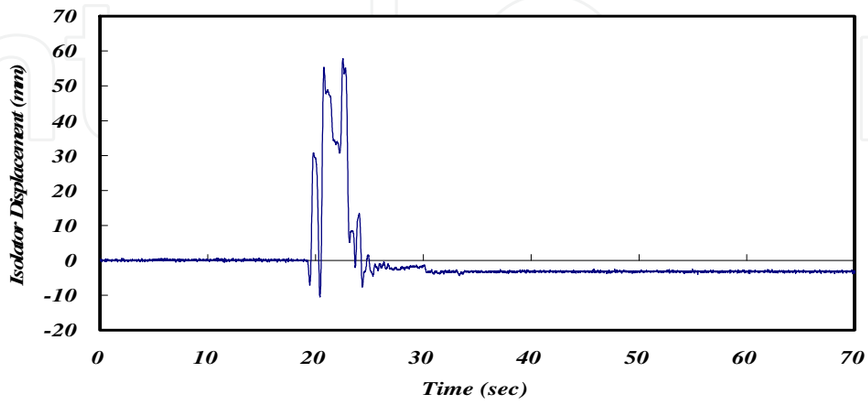

Fig. 39. Base isolator displacement of DO-FPS isolator at angle of 90° during 0.35 g Kobe ground motion

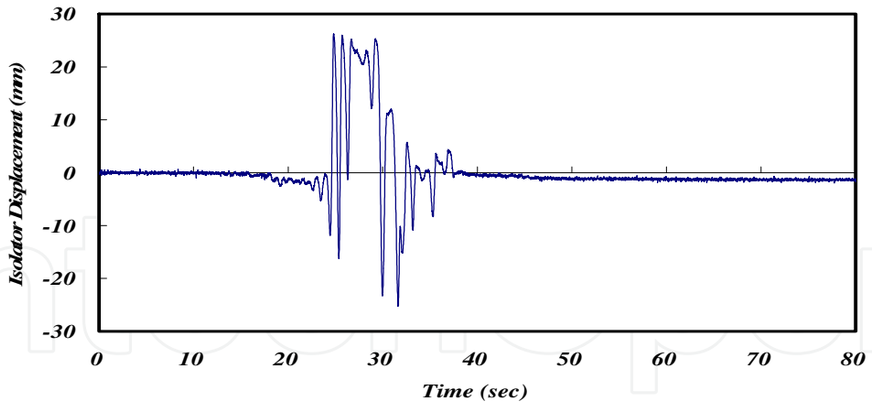

Fig. 40(a). Base isolator displacement of DO-FPS isolator at angle of 90° during 0.3 g Chi-Chi ground motion

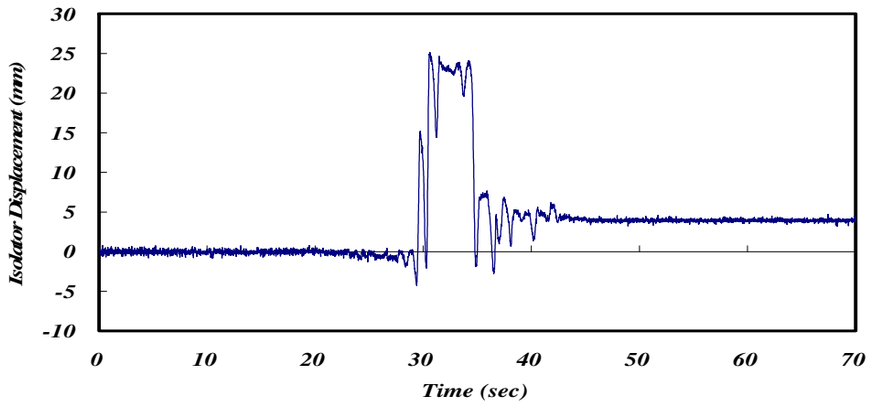

Fig. 40(b). Base isolator displacement of DO-FPS isolator at angle of 0° during 0.3 g Chi-Chi ground motion

As shown in Tables 1 and 2, the maximum roof accelerations of critical equipment have been reduced remarkably under various types of earthquakes. Therefore, the DO-FPS isolator can be recognized as an effective tool for upgrading the seismic resistance of high-technology facilities by isolating earthquake induced energy trying to impart into the equipment. This device also supplies significant damping for the isolation system through the frictional force resulting from the sliding motion of the slider on the sliding surface to reduce the isolator displacement and the bearing size.

4. Discussions

Earthquake proof technologies such as energy absorbing systems and base isolation systems have been accepted as powerful tools to protect structures and equipments from earthquake damage. At the same time, what we should bear in mind is that the design earthquakes utilized for estimating the performance of such technologies in safeguarding structures and equipments still leave room for future research. More recently, a new methodology based on

damages indices to obtain design earthquake loads for seismic-resistant design of traditional building structures was proposed by Moustafa (2011). The prerequisite for examining the efficiencies of the earthquake proof technologies in protecting building, bridge, and lifeline structures and equipments is having rational design earthquake loads associated with the occurrence and their characteristics (e.g. time, location, magnitude, frequency content and duration, etc.). More research efforts in this subject are needed to make this possible.

Max. Response	Roof Acceleration(g)			
Earthquake	Amplitude (PGA)	Fixed-Base Structure	Isolated Structure	Response Reduction
El Centro	0.2g	0.846	0.200	76.35%
	0.3g	1.492	0.239	83.96%
	0.4g	1.798	0.259	85.61%
Kobe	0.2g	0.589	0.187	68.26%
	0.3g	1.330	0.248	81.35%
	0.35g	1.687	0.274	83.75%
Chi-Chi	0.2g	0.605	0.177	70.79%
	0.3g	1.431	0.275	80.80%

Table 1. Maximum roof accelerations and earthquake efficiency for the DO-FPS isolated critical equipment at angle of 90°

Max. Response	Roof Acceleration(g)			
Earthquake	Amplitude (PGA)	Fixed-Base Structure	Isolated Structure	Response Reduction
El Centro	0.2g	0.827	0.285	65.53%
	0.3g	2.204	0.370	83.21%
	0.4g	3.723	0.472	87.31%
Kobe	0.2g	0.599	0.203	66.19%
	0.3g	1.345	0.293	70.39%
	0.35g	1.813	0.398	78.03%
Chi-Chi	0.2g	0.618	0.228	63.08%
	0.3g	1.451	0.282	80.56%

Table 2. Maximum roof accelerations and earthquake efficiency for the DO-FPS isolated critical equipment at angle of 0°

5. Conclusions

The isolators presented in this chapter, which provide damping as a result of the deformed material or the frictional force between the sliding interfaces, have rectified the drawbacks of the rolling ball isolation system, such as little damping provided by the system, highly concentrated stress produced by the rolling ball or cylindrical rod due to the small contact area between the rolling ball (or cylindrical rod) and the concave surfaces, and scratches and damage to the concave surfaces caused by the ball or cylindrical rod motions during earthquakes. The presented isolators not only effectively lengthen the natural period of the vibration sensitive equipment but also provide significant damping to reduce the bearing displacement and size and the protection to the contact area between the damped steel ball (or articulated slider) and the concave surface to prevent any damage or scratch on the concave surfaces. Further, the advanced isolators possess a stable mechanical behavior during the life span of service. In addition, the isolators can isolate energy induced by earthquakes to ensure the safety and functionality of the vibration sensitive equipment located in a building. It can be concluded from these studies that the presented isolators in this chapter, including the rolling and sliding types of isolators, exhibit excellent features for preventing vibration sensitive equipment from earthquake damage.

6. References

Alhan, C. and Gavin, H. P. (2005). Reliability of Base Isolation for the Protection of Critical Equipment from Earthquake Hazards. *Engineering Structures*, Vol. 27, 1435-1449.

Al-Hussaini, T. M.; Zayas, V. A. and Constantinou, M. C. (1994). *Seismic Isolation of Multi-story Frame Structures Using Spherical Sliding Isolation Systems*. NCEER Technical Report, NCEER-94-0007, National Center for Earthquake Engineering Research, State University of New York at Buffalo, NY.

Bakker, J. F. J. (1935). *Balance Block for Buildings*. US Patent No. 2014643.

Chung, L. L.; Yang, C. Y.; Chen, H. M. and Lu, L. Y. (2008). Dynamic Behavior of Nonlinear Rolling Isolation System. *Structural Control and Health Monitoring*, DOI: 10.1002/stc.305.

Cummings, F. D. (1930). *Building Construction (Quakeproof Building)*. US Patent No. 1761659.

Eberhard, M. O.; Baldridge, S.; Marshall, J.; Mooney, W. and Rix, G. J. (2010). *The MW 7.0 Haiti Earthquake of January 12, 2010: USGS/EERI Advance Reconnaissance Team Report*. Report 2010–1048, U.S. Department of the Interior, U.S. Geological Survey.

Fan, Y. C.; Loh, C. S.; Yang, J. N. and Lin, P. Y. (2008). Experimental Performance Evaluation of an Equipment Isolation Using MR Dampers. *Earthquake Engineering and Structural Dynamics*, DOI: 10.1002/eqe.844.

Fathali, S. and Filiatrault, A. (2007). *Experimental Seismic Performance Evaluation of Isolation/Restraint Systems for Mechanical Equipment, Part 2: Light Equipment Study*. Technical Report MCEER-07-0022, University at Buffalo, The State University of New York.

Fenz, D. M. and Constantinou, M. C. (2006). Behavior of the Double Concave Friction Pendulum Bearing. *Earthquake Engineering and Structural Dynamics*, Vol. 35, No. 11, 1403–1424.

Fenz, D. M. and Constantinou, M. C. (2008a). Spherical Sliding Isolation Bearings with Adaptive Behavior-Theory. *Earthquake Engineering and Structural Dynamics,* Vol. 37, No. 2, 168-183.

Fenz, D. M. and Constantinou, M. C. (2008b). *Mechanical Behavior of Multi-spherical Sliding Bearings.* Technical Report MCEER-08-0007, Multidisciplinary Center for Earthquake Engineering Research, State University of New York at Buffalo, NY.

Kanamori, H. (1978). Quantification of Earthquakes. *Nature*, Vol. 271, No. 5644, 411-414.

Kasalanati, A.; Reinhorn, A. M.; Constantinou, M. C. and Sanders, D. (1997). Experimental Study of Ball-in-cone Isolation System. *Proceedings of the structures congress XV*, *ASCE*, Vol. 2. Portland, Oregon, 1191–1195.

Kemeny, Z. A. (1997). *Ball-in-cone Seismic Isolation Bearing*. US Patent No. 5599106.

Kim, J. K. (2004). *Directional Rolling Pendulum Seismic Isolation Systems and Roller Assembly Therefore*. US patent No. 6725612, Filing date: March 11, 2002..

Kim, Y. S. and Yun, C. B. (2007). Seismic Response Characteristics of Bridges Using Double Concave Friction Pendulum Bearings with Tri-linear Behavior. *Engineering Structures*, Vol. 29, No. 11, 3082-3093.

Lin, T. W. and Hone, C. C. (1993). Base Isolation by Free Rolling Rods under Basement. *Earthquake Engineering and Structural Dynamics*, Vol. 22, 261–73.

Morgan, T. A. and Mahin, S. A. (2008). The Optimization of Multi-stage Friction Pendulum Isolators for Loss Mitigation Considering a Range of Seismic Hazard. In the *14th World Conference on Earthquake Engineering*, Beijing, China, Paper No. 11-0070.

Morgan, T. A. and Mahin, S. A. (2010). Achieving Reliable Seismic Performance Enhancement Using Multi-stage Friction Pendulum Isolators. *Earthquake Engineering and Structural Dynamics*, Vol. 39, 1443–1461.

Moustafa, A. (2011). Damage-Based Design Earthquake Loads for Single-Degree-Of-Freedom Inelastic Structures. *Journal of Structural Engineering*, *ASCE*, Vol. 137, No. 3, March, 2011, 456-467.

Naeim, F. and Kelly, J. M. (1999). *Design of Seismic Isolated Structures: from Theory to Practice*. John Wiley & Sons, ISBN: 0-471-14921-7, New York.

Penkuhn, A. L. K. (1967). *Three Point Foundation for Building Structures*. US Patent No. 3347002.

Rivin, E. I. (2003). *Passive Vibration Isolation*. The American Society of Mechanical Engineers, ISBN: 0-7918-0187-X.

Roussis, P. C. and Constantinou, M. C. (2005). *Experimental and Analytical Studies of Structures Seismically Isolated with an Uplift-restraint Isolation System*. Technical Report MCEER005-0001, Buffalo, NY.

Schär, F. (1910). *Foundation for Buildings*. US Patent No. 951028.

Skinner, R. I.; Robinson, W. H. and McVerry, G. H. (1993). *An Introduction to Seismic Isolation*. John Wiley & Sons, ISBN: 0-471-93433-X, New York.

Soong, T. T. and Dargush, G. F. (1997). *Passive Energy Dissipation Systems in Structural Engineering*. John Wiley & Sons, ISBN: 0-471-96821-8, New York.

Takewakin, I. (2009). *Building Control with Passive Dampers*. John Wiley & Sons, ISBN: 978-0-470-82491-7, Singapore.

Takewakin, I.; Murakami, S.; Fujita, K.; Yoshitomi, S. and Tsuji, M. (2011). The 2011 off the Pacific Coast of Tohoku Earthquake and Response of High-rise Buildings under Long-period Ground Motions. *Soil Dynamics and Earthquake Engineering*, doi:10.1016/j.soildyn. 2011.06.001.

Tsai, C. S. (2003). *Improved Structures of Base Isolation Systems*. Taiwan patent No. 207126, Publication Number: 00542278, Publication date: July 11, 2003, Application number: 091210175, Filing date: July 4, 2002 [in Chinese].

Tsai, C. S. (2004a). *Structure of an Anti-shock Device*. US Patent No. 6688051, Filing date: March 7, 2002.

Tsai, C. S. (2004b). *Structure of an Anti-shock Device*. US Patent No. 6820380, Filing date: Sept. 10, 2003.

Tsai, C. S. (2007). *Foundation Shock Eliminator*. US Patent No. 7237364, Filing Date: July 2, 2004.

Tsai, C. S. (2008a). *Foundation Shock Suppressor*. US Patent No. 7338035, Filing date: Dec. 9, 2004.

Tsai, C. S. (2008b). *Anti Shock Device*. US Patent No. 7409799, Filing date: Dec. 13, 2005.

Tsai, C. S.; Chiang, T. C. and Chen, B. J. (2003a). Finite Element Formulations and Theoretical Study for Variable Curvature Friction Pendulum System. *Engineering Structures*, Vol. 25, No. 14, 1719-1730.

Tsai, C. S.; Chiang, T. C. and Chen, B. J. (2003b). Seismic Behavior of MFPS Isolated Structure under Near-fault Earthquakes and Strong Ground Motions with Long Predominant Periods. In the *2003 ASME Pressure Vessels and Piping Conference*, *Seismic Engineering*, Cleveland, Ohio, U. S. A., J. C. Chen, Editor, Vol. 466, 73-79.

Tsai, C. S.; Chiang, T. C. and Chen, B. J. (2005a). Experimental Evaluation Piecewise Exact Solution for Predicting Seismic Responses of Spherical Sliding Type Isolated Structures. *Earthquake Engineering and Structural Dynamics*, Vol. 34, No. 9, 1027–1046.

Tsai, C. S.; Cheng, C. K.; Chen, M. J. and Yu, S. H. (2005b). Experimental Study of MFPS-isolated Sensitive Equipment. in the *2005 ASME Pressure Vessels and Piping Conference, Seismic Engineering,* C. S. Tsai, editor, Denver, Colorado, U.S.A., 8:11-18.

Tsai, C. S.; Lin, Y. C.; Chen, W. S.; Chen, M. J. and Tsou, C. P. (2006a). The Material Behavior and Isolation Benefits of Ball Pendulum System. in the *2006 ASME Pressure Vessels and Piping Conference, Seismic Engineering*, James F. Cory, editor, Vancouver, BC, Canada, Paper No. PVP2006-ICPVT11-93252.

Tsai, C. S.; Chen, W. S.; Yu, S. H. and Yang, C. T. (2006b). Shaking Table Tests of Critical Equipment with Simple Isolators. in the *2006 ASME Pressure Vessels and Piping Conference, Seismic Engineering*, James F. Cory, Editor, Vancouver, BC, Canada., July 23-27, No. PVP2006-ICPVT11-93250.

Tsai, C. S.; Chen, W. S.; Chiang, T. C. and Chen, B. J. (2006c). Component and Shaking Table Tests for Full-scale Multiple Friction Pendulum System. *Earthquake Engineering and Structural Dynamics,* Vol. 35, No. 11, 1653–1675.

Tsai, C. S.; Chen, W. S.; Chiang, T. C. and Lin, Y. C. (2007). Application of Direction Optimized-Friction Pendulum System to Seismic Mitigation of Sensitive Equipment. in the *2007 ASME Pressure Vessels and Piping Conference*, *Seismic Engineering*, Artin Dermenjian, editor, San Antonio, Texas, U.S.A., Paper No. PVP2007-26552.

Tsai, C. S.; Chen, W. S.; Lin, Y. C.; Tsou, C. P.; Chen, C. C. and Lin, C. L. (2008a). Shaking Table Tests of Motion Sensitive Equipment Isolated with Static Dynamics Interchangeable-Ball Pendulum System. In: the *14th World Conference on Earthquake Engineering*, Beijing, China, Paper No. 11-0010.

Tsai, C. S.; Lu, P. C.; Chen, W. S.; Chiang, T. C.; Yang, C. T. and Lin, Y. C. (2008b). Finite Element Formulation and Shaking Table Tests of Direction-Optimized Friction Pendulum System. *Engineering Structures*, Vol. 30, No. 9, 2321-2329.

Tsai, C. S.; Lin, Y. C. and Su, H. C. (2010a). Characterization and Modeling of Multiple Friction Pendulum Isolation System with Numerous Sliding Interfaces. *Earthquake Engineering and Structural Dynamics*, Vol. 39, No. 13, 1463–1491.

Tsai, C. S.; Lin, Y. C. and Su, H. C. (2010b). Seismic Responses of a Building Isolated with Multiple Friction Pendulum System Subjected to Multi-directional Excitations. In the *2010 ASME Pressure Vessels and Piping Conference, Seismic Engineering*, O'Brien, Cheryl C. (ed.), Bellevue, Washington, U. S. A., Paper No. PVP2010-25587.

Tsai, C. S.; Chen, W. S. and Chiang, T. C. (2010c). Experimental and Numerical Studies of Trench Friction Pendulum System. *Structural Engineering and Mechanics, An International Journal*, Vol. 34, No. 2.

Tsai, C. S. and Lin, Y. C. (2010d). Mechanical Characteristics and Modeling of Multiple Trench Friction Pendulum System with Multi-intermediate Sliding Plates. *International Journal of Aerospace and Mechanical Engineering*, Vol. 4, No. 1.

Tsai, C. S.; Lin, Y. C. and Su, H. C. (2010e). Characteristic and Modeling of multiple Direction Optimized-Friction Pendulum System with Numerous Sliding Interfaces Subjected to Multi-directional Excitations. In the *2010 ASME Pressure Vessels and Piping Conference, Seismic Engineering*, O'Brien, Cheryl C. (ed.), Bellevue, Washington, U. S. A., Paper No. PVP2010-25598.

Tsai, C. S.; Wang, Y. M. and Su, H. C. (2011a). Experimental Study of a Full Scale Building Isolated with Multiple Friction Pendulum System with Multiple Sliding Interfaces. In the *2011 ASME Pressure Vessels and Piping Conference*, *Seismic Engineering*, O'Brien, Cheryl C. (ed.), Baltimore, Maryland, U. S. A., Paper No. PVP2011-57352.

Tsai, C. S.; Hsueh, C. I. and Su, H. C. (2011b). Experimental Investigation on Performance of Multiple Direction-Optimized Friction Pendulum System with Multiple Sliding Interfaces in Mitigating Structural Responses during Earthquakes. In *the 2011 ASME Pressure Vessels and Piping Conference, Seismic Engineering*, O'Brien, Cheryl C. (ed.), Baltimore, Maryland, U. S. A., Paper No. PVP2011-57598.

Tsai, M. H.; Wu, S. Y.; Chang, K. C. and Lee, G. C. (2007). Shaking Table Tests of a Scaled Bridge Model with Rolling-type Seismic Isolation Bearings. *Engineering Structures*, Vol. 29, 694-702.

Touaillon, J. (1870). *Improvement in Buildings*. US Letters Patent No. 99973.

Wu, C. J. (1989). *Anti-earthquake Structure Insulating the Kinetic Energy of Earthquake from Buildings*. US Patent No. 4881350.

Zayas, V. A. (1987). *Earthquake Protective Column Support*. US Patent No. 4644714.

Zayas, V. A.; Low, S. S. and Mahin, S. A. (1987). *The FPS Earthquake Resisting System Report*. EERC Technical Report, UBC/EERC-87/01, University of California, Berkeley, CA.

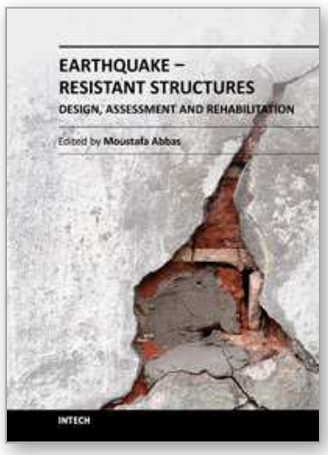

Earthquake-Resistant Structures - Design, Assessment and Rehabilitation

Edited by Prof. Abbas Moustafa

ISBN 978-953-51-0123-9
Hard cover, 524 pages
Publisher InTech
Published online 29, February, 2012
Published in print edition February, 2012

This book deals with earthquake-resistant structures, such as, buildings, bridges and liquid storage tanks. It contains twenty chapters covering several interesting research topics written by researchers and experts in the field of earthquake engineering. The book covers seismic-resistance design of masonry and reinforced concrete structures to be constructed as well as safety assessment, strengthening and rehabilitation of existing structures against earthquake loads. It also includes three chapters on electromagnetic sensing techniques for health assessment of structures, post earthquake assessment of steel buildings in fire environment and response of underground pipes to blast loads. The book provides the state-of-the-art on recent progress in earthquake-resistant structures. It should be useful to graduate students, researchers and practicing structural engineers.

InTech Europe
University Campus STeP Ri
Slavka Krautzeka 83/A
51000 Rijeka, Croatia
Phone: +385 (51) 770 447
Fax: +385 (51) 686 166
www.intechopen.com

InTech China
Unit 405, Office Block, Hotel Equatorial Shanghai
No.65, Yan An Road (West), Shanghai, 200040, China
中国上海市延安西路65号上海国际贵都大饭店办公楼405单元
Phone: +86-21-62489820
Fax: +86-21-62489821

IntechOpen